

1                                   **Responses of Arctic Black Carbon and Surface**  
2 **Temperature to Multi-Region Emission Reductions: an HTAP2**  
3 **ensemble modeling study**  
4  
5

6 **Na Zhao<sup>1</sup>, Xinyi Dong<sup>2</sup>, Kan Huang<sup>1\*</sup>, Joshua S. Fu<sup>3,4\*</sup>, Marianne Tronstad Lund<sup>5</sup>,**  
7 **Kengo Sudo<sup>6</sup>, Daven Henze<sup>7</sup>, Tom Kucsera<sup>8</sup>, Yun Fat Lam<sup>9</sup>, Mian Chin<sup>10</sup>, Simone**  
8 **Tilmes<sup>11</sup>**  
9

10 <sup>1</sup> Shanghai Key Laboratory of Atmospheric Particle Pollution and Prevention (LAP3), Department of  
11 Environmental Science and Engineering, Fudan University, Shanghai, China

12 <sup>2</sup> School of Atmospheric Science, Nanjing University, Nanjing, China

13 <sup>3</sup> Department of Civil and Environmental Engineering, The University of Tennessee, Knoxville,  
14 Tennessee, USA.

15 <sup>4</sup> Computational Earth Science Group, Computational Sciences and Engineering Division, Oak  
16 Ridge National Laboratory, Oak Ridge, Tennessee, USA.

17 <sup>5</sup> CICERO Center for International Climate and Environmental Research, Oslo, Norway

18 <sup>6</sup> Nagoya University, Furo-cho, Chigusa-ku, Nagoya, Japan

19 <sup>7</sup> Department of Mechanical Engineering, University of Colorado, Boulder, CO, USA

20 <sup>8</sup> Universities Space Research Association, Greenbelt, MD, USA

21 <sup>9</sup> Department of Geography, The University of Hong Kong, HKSAR, China

22 <sup>10</sup> Earth Sciences Division, NASA Goddard Space Flight Center, Greenbelt, MD, USA

23 <sup>11</sup> Atmospheric Chemistry Observations and Modeling Laboratory, National Center for Atmospheric  
24 Research, Boulder, Colorado, USA  
25

26 Correspondence: huangkan@fudan.edu.cn; jsfu@utk.edu

27 **ABSTRACT**

28 Black carbon (BC) emissions play an important role in regional climate change of the Arctic. It is  
29 necessary to pay attention to the impact of long-range transport from regions outside the Arctic as  
30 BC emissions from local sources in the Arctic were relatively small. The Task Force Hemispheric  
31 Transport of Air Pollution Phase2 (HTAP2) set up a series of simulation scenarios to investigate the  
32 response of BC in a given region to different source regions. This study investigated the responses of  
33 Arctic BC concentrations and surface temperature to 20% anthropogenic emission reductions from  
34 six regions in 2010 within the framework of HTAP2 based on ensemble modeling results. Emission  
35 reductions from East Asia (EAS) had most (monthly contributions: 0.2 - 1.5 ng m<sup>-3</sup>) significant  
36 impact on the Arctic near surface BC concentrations while the monthly contributions from Europe

37 (EUR), Middle East (MDE), North America (NAM), Russia-Belarus-Ukraine (RBU), and South Asia  
38 (SAS) were  $0.2\text{--}1.0\text{ ng m}^{-3}$ ,  $0.001\text{--}0.01\text{ ng m}^{-3}$ ,  $0.1\text{--}0.3\text{ ng m}^{-3}$ ,  $0.1\text{--}0.7\text{ ng m}^{-3}$ ,  $0.0\text{--}0.2\text{ ng m}^{-3}$ ,  
39 respectively. The responses of the vertical profiles of the Arctic BC to the six regions were found to  
40 be different due to multiple transport pathways. Emission reductions from NAM, RBU, EUR, and  
41 EAS mainly influenced the BC concentrations in low troposphere of the Arctic, while most of the BC  
42 in the upper troposphere of the Arctic derived from SAS. The response of the Arctic BC to emission  
43 reductions of six source regions became less significant with the increase of the latitude. The benefit  
44 of BC emission reductions in terms of slowing down surface warming in the Arctic was evaluated by  
45 using Absolute Regional Temperature-change Potential (ARTP). Compared to the response of global  
46 temperature to BC emission reductions, the response of Arctic temperature was substantially more  
47 sensitive, highlighting the need for curbing global BC emissions.

## 48 **1. Introduction**

49 Black carbon (BC) is one of the short-lived climate forcers (SLCFs, AMAP, 2015) and was regarded  
50 as the second largest contributor to global warming, only inferior to carbon dioxide (Bond et al.  
51 2013). BC over the Arctic can perturb the radiation balance in a number of ways. Direct aerosol  
52 forcing occurred through absorption or scattering of solar (shortwave) radiation. BC is the most  
53 efficient atmospheric particulate species at absorbing visible light (Bond et al., 2013), the added  
54 atmospheric heating will subsequently increase the downward longwave radiation to the surface and  
55 warm the surface (AMAP, 2011). Radiative forcing by BC can also result from aerosol-cloud  
56 interactions that affected cloud microphysical properties, albedo, extent, lifetime, and longwave  
57 emissivity (Twomey 1977; Garrett and Zhao 2006). BC has an additional forcing mechanism after  
58 depositing onto snow and ice surfaces (Clarke and Noone, 1985). The surface albedo of snow and ice  
59 could be reduced and further enhanced the absorption of solar radiation at the surface. In the Arctic,  
60 surface temperature responses were strongly linked to surface radiative forcing as the stable  
61 atmosphere of the region prevented rapid heat exchange with the upper troposphere (Hansen and  
62 Nazarenko, 2004).

63 The Arctic has been warming twice as rapidly as the world in the past fifty years, and has  
64 experienced significant changes in its ice and snow covers as well as permafrost (AMAP, 2017).

65 Reductions of carbon dioxide emissions are the backbone of any meaningful effort to mitigate  
66 climate forcing. But even if significant reductions of carbon dioxide are made, slow down of the  
67 temperature rise in the Arctic and the sea level rise caused by the melting of glaciers may not be  
68 achieved in time. Hence, the goal of slowing down the deterioration of the Arctic may best be  
69 achieved by also targeting at shorter-lived climate forcing agents, especially those that could impose  
70 appreciable surface forcing and trigger regional-scale climate feedbacks pertaining to the melting of  
71 sea ice and snow. Modelling studies by UNEP/WMO (2011) and Stohl et al. (2015) suggested that  
72 the climate response of SLCFs mitigation was strongest in the Arctic region. AMAP (2011 and 2015)  
73 as well as Sand et al. (2016) demonstrated that per unit of emission reductions of SLCFs in the  
74 Northern areas had the largest temperature response on the Arctic, with the Nordic countries  
75 (Denmark, Finland, Iceland, Norway, and Sweden) and Russia having the largest impact compared to  
76 other Arctic countries such as the United States and Canada.

77 The few studies that investigated specific regional aerosol forcing (Shindell and Faluvegi, 2009;  
78 Shindell et al., 2012; Teng et al., 2012) typically used a single climate model at a time to investigate  
79 the climate response to idealized, historical, or projected forcing. However, different models varied  
80 considerably in the representation of aerosols and radiative properties, resulting in large uncertainties  
81 in simulating the aerosol radiative forcing (Myhre et al., 2013b; Shindell et al., 2013). When  
82 investigating the climate response to regional emissions, such uncertainties were likely to be  
83 confounded even further by the variability between models in regional climate and circulation  
84 patterns and variation in the global and regional climate sensitivity (the amount of simulated  
85 warming per unit radiative forcing). Hence, the Task Force Hemispheric Transport of Air pollution  
86 Phase2 (HTAP2, <http://www.htap.org/>) incorporating multiple global models can avoid the great  
87 uncertainty of single model to a certain degree, with the aim to improve model estimates of the  
88 impacts of intercontinental transport of air pollutants on climate, ecosystems, and human health  
89 (Galmarini et al., 2017). To date, the HTAP2 results have been explored from a variety of scientific  
90 and policy-relevant perspectives. For instance, by comparing against observations, sulfur and  
91 nitrogen depositions during HTAP2 had been significantly improved compared to HTAP1. From  
92 2001 to 2010, the global nitrogen deposition increased 7% while the global sulfur deposition  
93 decreased 3% (Tan et al., 2018a). The significant impacts of hemispheric transport on the deposition  
94 were specifically focused and the deposition over the coastal regions was more sensitive to

95 hemispheric transport than the non-coastal continental regions (Tan et al., 2018b). Jonson et al. (2018)  
96 assessed the contributions from different world regions to European ozone levels and contributions  
97 from the non-European regions were mostly from North America and eastern Asia, larger than those  
98 from European emissions. Hogrefe et al. (2018) found that the simulated ozone over the continental  
99 US varied very differently by digesting boundary conditions from four hemispheric or global models.  
100 The impact of emission changes from six major source regions on global aerosol direct radiative  
101 forcing was estimated (Stjern et al., 2016). In the local source regions, the radiative forcing  
102 associated with  $\text{SO}_4^{2-}$  was strengthened (25%) while that from BC was weakened (37%) due to a  
103 20% emission reduction. Liang et al. (2018) estimated global air-pollution-related premature  
104 mortality from exposure to  $\text{PM}_{2.5}$  and ozone and the interregional transport lead to more deaths  
105 through changes in  $\text{PM}_{2.5}$  than in  $\text{O}_3$ . However, the source region contributions to Arctic BC and the  
106 spread among multi-model results have been rarely explored from the perspective of HTAP2  
107 initiative.

108 This study aims to investigate the responses of Arctic BC concentrations and surface temperature  
109 to 20% anthropogenic emission reductions from different regions in the Northern Hemisphere (NH).  
110 A comparison of six global modeling works within the framework of HTAP2 experiments for the  
111 Arctic region in 2010 was presented. The ensemble modeling results were used to apportion the  
112 contribution from different source regions to the near-surface and vertical black carbon in the Arctic.  
113 In addition, the Arctic surface temperature responses to the emission reductions were estimated.

## 114 **2. Methodology**

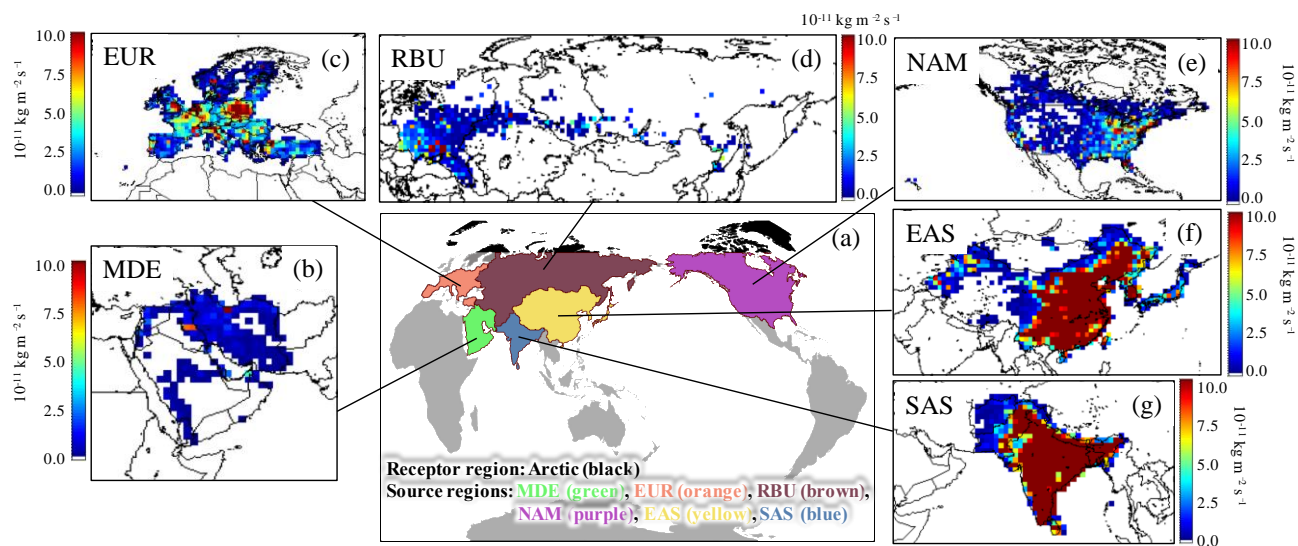
### 115 **2.1 HTAP2 experiments**

116 HTAP2 developed a harmonized emissions database covering all countries and the major sectors for  
117 global and regional modeling from 2008 to 2010. The emissions database was obtained from the  
118 nationally reported emissions (e.g., National Emission Inventory for the United States), the regional  
119 scientific inventories (e.g., European Monitoring and Evaluation Programme (EMEP), Netherlands  
120 Organisation for Applied Scientific Research (TNO) for Europe, Model Inter-Comparison Study for  
121 Asia, MICS–Asia III), and the Emissions Database for Global Atmospheric Research data  
122 (EDGARv4.3) for the rest of the world (mainly South America, Africa, Russia, and Oceania).

123 Biomass burning emissions were not prescribed in HTAP2. Temporal resolution of data sources was  
 124 monthly, and thus the HTAP2 emission inventory provided harmonized emission data with monthly  
 125 resolution for all the air pollutants including BC. It should be noted that the emissions of  
 126 international shipping and international aviation in HTAP2 were considered constant over the year. It  
 127 was recommended that modeling groups used the Global Fire Emissions Database (GFED4,  
 128 <http://globalfiredata.org/>) with a temporal resolution of daily or 3-hour intervals. The detailed  
 129 information of different regional inventories can be found in Janssens–Maenhout et al. (2015).

130 Emission perturbations were conducted in sensitivity simulations to investigate the response of  
 131 various air pollutants in a given region to different source regions. In this study, the Arctic region was  
 132 the targeted receptor region of interest. Six source regions in HTAP2 experiments, namely, East Asia  
 133 (EAS), Europe (EUR), Middle East (MDE), North America (NAM), Russia–Belarus–Ukraine (RBU),  
 134 and South Asia (SAS) were selected to demonstrate their influences on the BC concentrations over  
 135 the Arctic region (Figure 1a). Two emission scenarios were designed for the HTAP2 simulation to  
 136 explore the source/receptor relationships, i.e. the base scenario (BASE) with no emission reduction,  
 137 and the control scenario (EASALL, EURALL, MDEALL, NAMALL, RBUALL, and SASALL)  
 138 with 20% reduction of all anthropogenic emissions in six regions respectively.

139



140

141 **Figure 1.** (a) The sketch map of receptor and source regions. (b)–(g) Spatial distributions of 20% reduction of  
 142 annual BC emission in the six source regions in 2010. MDE: Middle East; EUR: Europe; RBU:  
 143 Russia–Belarus–Ukraine; NAM: North America; EAS: East Asia; SAS: South Asia. The unit legends from (b) to (g)  
 144 are the same of  $10^{-11} \text{ kg m}^{-2} \text{ s}^{-1}$ .

145 **2.1.1 Anthropogenic emission reductions of BC in HTAP2**

146 Anthropogenic BC emission sectors included power plants, industries, transportation, shipping,  
 147 aviation, agriculture, and residential sectors. The emission inventory had a monthly temporal  
 148 resolution and a spatial resolution of  $0.1^\circ \times 0.1^\circ$ . The total anthropogenic emissions and 20%  
 149 emission reductions of BC in six source regions of HTAP2 in 2010 are presented in Table 1. The  
 150 higher BC emission reductions were found in the EAS and SAS with the values of 355.6 and 232.5  
 151 Gg yr<sup>-1</sup>, respectively, while were much lower in the MDE and RBU with the values of 5.3 and 18.6  
 152 Gg yr<sup>-1</sup>, respectively. The BC emission reductions in the EAS, EUR, and RBU showed significant  
 153 monthly variations with higher values from November to March, while the monthly variations were  
 154 not obvious in the MDE, NAM, and SAS.

155

156 **Table 1.** 20% emission reductions and total anthropogenic emissions of BC in different regions of HTAP2 in 2010.  
 157 (Unit: Gg yr<sup>-1</sup>).

Regions	Total anthropogenic emissions	20% Emission Reductions												2010
		Jan	Feb	Mar	Apr	May	Jun	Jul	Aug	Sep	Oct	Nov	Dec	
EAS <sup>a</sup>	1778.1	46.4	35.6	33.0	24.1	23.9	24.0	24.0	23.6	23.5	25.0	31.4	41.0	355.6
EUR <sup>b</sup>	326.3	6.7	6.4	7.2	6.5	5.3	4.9	4.0	3.7	4.4	5.2	5.3	5.7	65.3
MDE <sup>c</sup>	26.7	0.4	0.4	0.5	0.5	0.5	0.4	0.4	0.4	0.4	0.5	0.5	0.5	5.3
NAM <sup>d</sup>	310.8	5.2	5.1	5.3	5.1	5.1	5.2	5.3	5.3	5.1	5.1	5.1	5.2	62.2
RBU <sup>e</sup>	93.0	2.0	1.9	1.9	1.7	1.4	1.3	1.0	1.1	1.2	1.6	1.7	1.8	18.6
SAS <sup>f</sup>	1162.7	20.4	19.1	19.7	18.9	19.2	18.9	19.2	19.2	19.0	19.3	19.2	20.4	232.5
All	3697.6	81.2	68.5	67.6	56.8	55.4	54.7	53.9	53.3	53.6	56.7	63.2	74.6	739.5
Global	5492.9	110.6	86.2	92.8	103.9	98.7	97.2	86.8	85.4	85.4	84.2	83.3	83.9	1098.6

158 <sup>a</sup> East Asia. <sup>b</sup> Europe. <sup>c</sup> Middle East. <sup>d</sup> North America. <sup>e</sup> Russia–Belarus–Ukraine. <sup>f</sup> South Asia.

159 Figure 1b–g illustrates the spatial distribution of the 20% reductions of annual BC emissions in six  
 160 source regions in 2010. It can be found that the most intense reductions of BC emissions in EAS and  
 161 SAS were concentrated in East China and India, respectively, which were mainly attributed to  
 162 emissions from residential sectors, followed by transportation and industries. The BC emission  
 163 reductions of EUR were widely distributed with high values in central Europe, with residential and  
 164 transportation sectors accounting for the largest proportion. The reductions near the Arctic circle  
 165 could be found in the north of EUR, NAM, and RBU. For MDE, most BC was emitted from Iran,  
 166 which located in the northeast of this region. Overall, the spatial pattern of BC emission reductions in  
 167 six regions was closely related to the spatial distribution of the human population.

168 **2.1.2 Model description**

169 Considering that the simulations should cover all months of 2010 and all emission source regions,  
 170 five global models (i.e. CAMchem, CHASER\_re1, GEOS-Chem, GOCART–v5, and Oslo CTM3–v2)  
 171 were incorporated to simulate the responses of BC concentrations in the Arctic to 20% BC emission  
 172 reductions from EAS, EUR, MDE, NAM, RBU, and SAS, respectively. The brief information of  
 173 model configurations is listed in Table 2. As required by HTAP2, all simulations should include a  
 174 spin-up time of 6 months prior to the period of interest. The outputs from all models are available  
 175 upon request from <http://aerocom.met.no>. The time resolution of the outputs used in this study is  
 176 monthly for all models, although models were run at a finer resolution (e.g., daily or hourly). The  
 177 model outputs for air pollutants were originally provided in the unit of mass mixing ratio (MMR, kg  
 178 kg<sup>-1</sup>). To facilitate comparison between model and observation and further data analysis, we  
 179 converted the original units into ng m<sup>-3</sup> based on the ideal gas law (Aamaas et al., 2017).

180

181 **Table 2.** Configurations of models used in this study

Models	Meteorological field	Horizontal resolution	Vertical layers	Convection	Reference
CAMchem	GEOS5 v5.2	1.9° × 2.5°	56	Zhang–McFarlane approach for deep convection	Lamarque et al., 2012; Tilmes et al., 2016
CHASER_re1	ERA-Interim and HadISST	2.8° × 2.8°	32	CCSR/NIES AGCM for advection, convection, and other subgrid–scale mixing	Sudo et al., 2002; Takashi et al., 2018
GEOS-Chem	GEOS–5 (MERRA)	2.0° × 2.5°	47	Convective transport is computed from the convective mass fluxes in the meteorological archive	Henze et al., 2007
GOCART–v5	MERRA	1.3° × 1.0°	72	MERRA for moist convection, Arakawa–Schubert (RAS) algorithm for GCTM	Chin et al., 2000
Oslo CTM3–v2	ECMWF–IFS	2.8° × 2.8°	60	Tiedke mass flux scheme for deep convection	Søvde et al., 2012; Lund et al., 2018

182 **2.2 Calculation of the temperature response to BC emissions reduction**

183 The climate effects of air pollutants have been the focus of climate change research since the last  
 184 century (IPCC, 1990; IPCC, 2001). In the last few years, the metrics for estimating this kind of effect  
 185 have been constantly improving (Shindell et al., 2012; Bond et al., 2013; Smith and Mizrahi, 2013;

186 Stohl et al., 2015). The Intergovernmental Panel on Climate Change (IPCC) used the Global  
187 Warming Potential (GWP) as a method for comparing the potential climate impact of emissions of  
188 different greenhouse gases (IPCC, 1990). GWP is the time-integrated radiative forcing due to a pulse  
189 emission of a given species, over some given time horizon (commonly 20, 100, or 500 years) relative  
190 to a pulse emission of carbon dioxide. GWP does not purport to represent the impact of air pollutant  
191 emissions on temperature. Although a short-lived climate pollutant (SLCP) could have the same  
192 GWP as a long-lived climate pollutant, identical (in mass terms) pulse emissions could cause a  
193 different temperature change at a given time, because long-lived climate pollutants accumulate in the  
194 climate system while short-lived climate pollutants can be broken down by various processes.  
195 Consequently, warming caused by long-lived climate pollutants is determined by total cumulative  
196 emissions to date, while the warming due to short-lived climate pollutants is determined more by the  
197 current rate of emissions in any given decade and depends much less on historical emissions. This  
198 means the importance of SLCP emissions is often overstated based on GWP. Shine et al. (2005)  
199 proposed the Global Temperature Change Potential (GTP) as a replacement for GWP to represent the  
200 global-mean surface temperature change for both a pulse emission ( $GTP_P$ ) and a sustained change in  
201 emissions ( $GTP_S$ ) of a given air pollutant. The distinction between  $GTP_P$  and  $GTP_S$  avoids the  
202 overestimation of GWP for the short-lived climate pollutants. Even for a uniform forcing, there will  
203 be differences of spatial patterns in the temperature response. Regional Temperature-change Potential  
204 (RTP) (Shindell and Faluvegi, 2010) was applied to analyze the temperature response on the regional  
205 scale, since both GWP and GTP focused on the global scale. The GWP, GTP, and RTP were  
206 normalized to the corresponding effect of CO<sub>2</sub> as the Absolute Global Warming Potential (AGWP),  
207 Absolute Global Temperature Change Potential (AGTP), and Absolute Regional Temperature-change  
208 Potential (ARTP), respectively. AGWP represented the absolute forms of radiative forcing. AGTP  
209 and ARTP represented the absolute forms of temperature perturbation. The ARTP provide additional  
210 insight into the spatial pattern of temperature response to inhomogeneous forcings beyond that  
211 available from traditional global metrics. Very few metrics have attempted to examine sub-global  
212 scales thus far, though some have used local information with non-linear global damage metrics  
213 (Shine et al., 2005a; Lund et al., 2012). Shindell et al. (2012) indicated that the forcing/response  
214 portion of the ARTP appeared to be relatively robust across models.

215 ARTPs is more suitable for this study to calculate the temperature response, considering that the



216 research object is BC with short lifetime and focus on regional impact of the BC emission reductions  
 217 on temperature changes in the Arctic. For SLCFs with atmospheric lifetimes much shorter than both  
 218 the time horizon of the ARTP and the response time of the climate system, the general expression for  
 219 the ARTP following a pulse emission of BC ( $E$ ) in region  $r$  which leads to a response in latitude band  
 220  $m$  is as follows (Fuglestad et al., 2010; Collins et al., 2013; Aamaas et al., 2017):

$$221 \quad \text{ARTP}_{r, m, s}(H) = \sum_l \frac{F_{l, r, s}}{E_{r, s}} \times \text{RCS}_{l, m} \times \text{R}_T(H) \quad (1)$$

222  $F_{l, r, s}$  (in  $\text{W m}^{-2}$ ) is the radiative forcing in latitude band  $l$  due to emission in region  $r$  in season  $s$  as  
 223 a function after the pulse emission  $E_{r, s}$  (in Tg). Even though our estimates are based on seasonal  
 224 emissions, the temperature responses calculated are annual means. Shindell and Faluvegi (2009)  
 225 analyzed BC climate effect in four different latitudes: southern mid-high latitudes ( $90^\circ\text{S}$ – $28^\circ\text{S}$ ),  
 226 tropics ( $28^\circ\text{S}$ – $28^\circ\text{N}$ ), northern mid-latitudes ( $28^\circ\text{N}$ – $60^\circ\text{N}$ ), and the Arctic ( $60^\circ\text{N}$ – $90^\circ\text{N}$ ), which gives  
 227 a better estimate of the global temperature response as it accounts for varying efficacies with latitude.  
 228 The  $\text{RCS}_{l, m}$  is a matrix of regional response coefficients based on the RTP concept (unitless; Collins  
 229 et al., 2013). As these response coefficients are normalized here, they contain no information on  
 230 climate sensitivity, only the relative regional responses in the different latitude bands. The global  
 231 climate sensitivity is included in the impulse response function  $\text{R}_T$ , which is a temporal temperature  
 232 response to an instantaneous unit pulse of RF (in  $\text{K m}^2 \text{W}^{-1}$ ). This paper refers to the ARTP values in  
 233 Aamaas et al. (2017). Aamaas et al. (2017) applies two refinements of the forcing-response  
 234 coefficients for radiative forcing occurring in the Arctic: one for the aerosol effects in the atmosphere  
 235 (Shindell and Faluvegi, 2010; Lund et al., 2014) and another for the effects due to BC on snow  
 236 (Flanner, 2013). The ARTP in this study estimated of the direct effect in the Arctic included both the  
 237 direct radiative forcing from outside the Arctic and within the Arctic, while the ARTP of the  
 238 semi-direct effect in the Arctic was due to the semi-direct radiative forcing from outside the Arctic.  
 239 The contribution by radiative forcing within the Arctic to Arctic temperature changes considered the  
 240 vertical profile of BC concentrations as both  $F_{\text{Arctic}, r, s}$  and  $\text{RCS}_{\text{Arctic}, \text{Arctic}}$  have a dependence on the  
 241 height of the BC (Lund et al., 2014; Lund et al., 2017). The total response in the Arctic was the sum  
 242 of the contributions from BC forcing outside of the Arctic and inside of the Arctic.

243 Regional temperature responses at time  $t$  of an emission  $E(t)$  can be calculated with these ARTP  
 244 values by a convolution (Aamaas et al., 2016). The temperature response is as follows:

245 
$$\Delta T_{r, m, s, t}(t) = \int_0^t E_{r, s, t}(t') \times ARTP_{r, m, s, t}(t-t') dt \quad (2)$$

246  $\Delta T_{r, m, s, t}$  refers to the decrease of the Arctic or global surface temperature after 20, 100, or 500 years  
247 to 20% BC emission reductions of six regions (namely EAS, EUR, MDE, NAM, RBU, and SAS) in  
248 the framework of HTAP2 either during summer or winter in this paper.

### 249 **3. Results and Discussion**

#### 250 **3.1 Model evaluation**

251 To evaluate the model performance from all five models, the monthly simulated surface BC  
252 concentrations of the BASE scenario were compared with the observations at four monitoring sites in  
253 the Arctic Circle in 2010. The locations of the four sites, including Alert (82.5°N, 62.3°W) in Canada,  
254 Barrow (71.3°N, 156.6°W) in Alaska, Tiksi (71.59°N, 128.92°E) in Russia, and Zeppelin (78.9°N,  
255 11.9°E) in Norway, are plotted in Figure S1 in the Supporting Information.

256 Metrics (Text S1) including correlative coefficient (COR), normalized mean bias (NMB),  
257 normalized mean error (NME), mean bias (MB), and mean absolute error (MAE) were selected for  
258 evaluating the model performance in this study (U.S. EPA, 2007) In addition to the evaluation for  
259 each single model, the multi-model ensemble mean (calculated as the average of all participating  
260 models) was also evaluated. The statistical results are listed in Table 3 and Table S1. A comparison  
261 between the monthly variations of simulated and observed BC concentrations is shown in Figure S2  
262 (a).

263 The correlations of the simulated BC concentrations among different models were moderate to  
264 high with CORs ranging from 0.33 to 0.98 (Table S1), suggesting the temporal variations of different  
265 models were relatively consistent. Overall, CAMchem, GEOS-Chem, GOCART-v5, and Oslo  
266 CTM3-v2 underestimated the near-surface BC (Figure S2a), which may be attributed to an  
267 underestimation of BC emissions, e.g., gas flaring (Huang et al., 2014, 2015; Stohl et al., 2013) and  
268 shipping emissions (Marelle et al., 2016). Also, appropriate temporal allocation of BC emissions  
269 from residential combustion was another important factor governing the model performance (Stohl et  
270 al., 2013). However, the simulated BC surface concentrations from CHASER\_re1 were higher than

271 those of the other four models and observations (Figure S2a), which mainly due to their slow BC  
272 aging-rate in remote/polar regions (Sudo et al., 2015).

273 Table 3 shows the model performances at the four Arctic sites. No single model could reproduce  
274 the BC concentrations in the Arctic well, and models performed differently at different monitoring  
275 sites. Relatively good agreement between the observation and models was found at Zeppelin, with  
276 CORs, NME, MB, and MAE of 0.59–0.83, 38.59%–142.64%, –13.53–14.97 ng m<sup>-3</sup>, and 5.40–14.97  
277 ng m<sup>-3</sup> among the five models, respectively. The best correlation (0.83) was found at Zeppelin from  
278 Oslo CTM3, while the smallest NMB (38.59%) and MAE (5.40 ng m<sup>-3</sup>) were found at Zeppelin from  
279 GOCART. On the contrary, the simulated BC concentrations didn't agree so well with observations  
280 at the other three sites with even negative COR values in some models (e.g., CAMchem, and  
281 CHASER\_re1), which may be explained by the uncertainties in emission inventory, the bias in the  
282 meteorological simulations, and chemical mechanisms (Miao et al., 2017; Zhang et al., 2019). All  
283 models, except Oslo CTM3, overestimated the BC concentrations in Barrow in July (Figure S2a),  
284 mainly due to the large contributions of biomass burning from Siberia in the simulations caused by  
285 overestimations of emissions and/or too little removal during transport (Sobhani et al., 2018).

286 The vertical profiles of simulated BC concentrations of the BASE simulation were also compared  
287 with aircraft measurements from HIAPER Pole-to-Pole Observations (HIPPO) during 24 March–16  
288 April 2010 (Figure S2b). Different from comparison between observed and simulated BC  
289 concentrations near the surface, the vertical profiles of BC concentrations were overestimated by  
290 most models. As the aircraft ascended and descended along each flight track, BC concentrations from  
291 HIPPO varied with time, latitude, longitude, and altitude. However, most of the simulation results of  
292 HTAP2 were provided in the temporal resolution of monthly, simulation and observation results  
293 cannot be exactly matched. This partly explained the difference between the simulations and  
294 observations. Overall, currently no single model could reproduce the BC concentrations over  
295 different regions of the Arctic well. There is a number of reasons responsible for this. First, the BC  
296 emission inventory in the Arctic is not well understood due to lacking of local activity data and  
297 emission factors, e.g. gas flaring in the oil and gas production fields, biofuel combustion, non-road  
298 transportation, etc. Secondly, the lifetime of BC in the atmosphere is sensitive to its wet deposition  
299 rates. However, different models have divergent treatment of wet scavenging parameterizations,  
300 which may be not representative in the Arctic region and could result in the simulated BC

301 concentrations ranging between several magnitudes. The mechanism of BC sinks is still not well  
 302 understood in the Arctic. Last but not the least, almost all the global models used the  
 303 latitude/longitude projection which has very large distortions over the polar regions and this may also  
 304 affect the ability of global models simulating the air pollutants over the Arctic region.

305 Although the single model didn't reproduce the BC concentrations in the Arctic well, the  
 306 consistency of the model ensemble mean with the observation was improved to some extent. The  
 307 NME and MAE of model ensemble mean was closer to zero compared with the single model.  
 308 Therefore, to reduce the bias from one single model, the multi-model ensemble mean was used for  
 309 further analysis.

310

311 **Table 3** Comparison of the simulations and observations of monthly surface BC concentrations at Alert, Barrow,  
 312 Tiksi, and Zeppelin in 2010.

Parameters	Sites	CAMchem	CHASER_re1	GEOS-Chem	GOCART-v5	Oslo CTM3-v2	Model ensemble mean
COR <sup>a</sup>	Alert	-0.24	-0.22	0.35	0.20	-0.24	-0.10
	Barrow	-0.28	-0.08	0.06	0.00	0.01	-0.06
	Tiksi	-0.19	0.05	0.50	0.48	0.41	0.11
	Zeppelin	0.72	0.59	0.80	0.76	0.83	0.73
NMB <sup>b</sup> (%)	Alert	-86.75	115.06	-57.81	-34.31	-92.38	-9.21
	Barrow	-38.43	104.10	-38.95	-8.18	-75.58	4.37
	Tiksi	-82.03	10.31	-69.76	-67.34	-84.82	-46.79
	Zeppelin	-79.93	142.64	-45.57	-9.81	-75.98	8.63
NME <sup>c</sup> (%)	Alert	86.75	151.30	66.37	70.77	92.38	74.69
	Barrow	72.07	124.44	69.50	84.20	75.58	72.12
	Tiksi	82.03	64.55	70.16	68.82	84.82	60.81
	Zeppelin	79.93	142.64	45.57	38.59	75.98	42.06
MB <sup>d</sup> (ng m <sup>-3</sup> )	Alert	-29.03	11.08	-21.41	-16.07	-30.16	-12.81
	Barrow	-22.13	15.35	-19.10	-11.12	-30.40	-9.44
	Tiksi	-55.99	-17.28	-48.51	-48.16	-56.26	-40.64
	Zeppelin	-13.53	14.97	-8.19	-3.59	-12.45	-1.44
MAE <sup>e</sup> (ng m <sup>-3</sup> )	Alert	29.03	31.05	22.85	22.23	30.16	23.56
	Barrow	29.01	28.91	26.71	30.30	30.40	25.22
	Tiksi	55.99	37.06	48.60	48.49	56.26	43.73
	Zeppelin	13.53	14.97	8.19	5.40	12.45	4.95

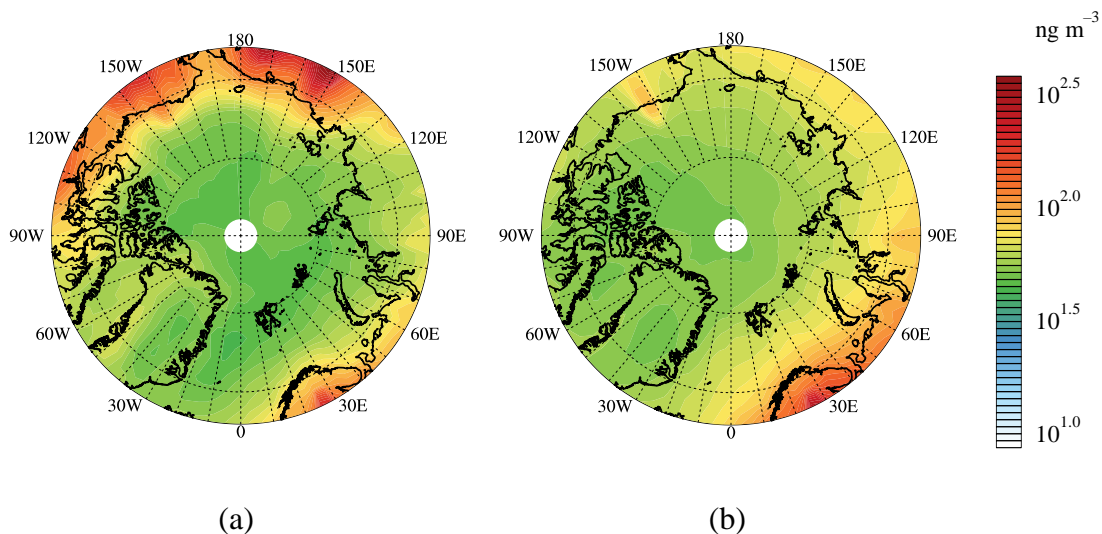
313 <sup>a</sup> Correlative coefficient. <sup>b</sup> Normalized mean bias. <sup>c</sup> Normalized mean error. <sup>d</sup> Mean bias. <sup>e</sup> Mean absolute error.

## 314 **3.2 Near-surface BC concentrations in the Arctic**

315 Before analyzing the responses of Arctic BC to emission reductions, it is necessary to understand the  
316 spatial-temporal distribution of BC concentrations in the Arctic region. In this study, months from  
317 May to October were defined as summer and November to April were defined as winter due to the  
318 special geographical location of the Arctic (Aamaas et al., 2017).

319 Spatial distributions of Arctic near surface BC concentrations in summer and winter simulated  
320 from each model are showed in Figure S4. BC simulated by CHASER\_re1 showed relatively high  
321 concentrations over the whole Arctic, followed by GEOS-chem and GOCART-v5, while those  
322 simulated by Oslo CTM3-v2 and CAMchem were lower. The difference of simulated BC  
323 concentrations between land and ocean was more obvious in summer than that in winter, especially  
324 for GEOS-chem and GOCART-v5. The mean BC concentrations from the ensemble models near the  
325 surface Arctic (66–90°N) were 18.6 ng m<sup>-3</sup> in summer and 16.6 ng m<sup>-3</sup> in winter in 2010,  
326 respectively. Figure 2 shows that the BC concentrations over the polar sea ice region in winter were  
327 higher than that in summer. The coverage of the polar dome expanded more southward in winter  
328 (Bozem et al., 2019; Law and Stohl, 2007), allowing more BC from lower latitudinal regions to be  
329 transported into the Arctic. Turbulent exchange and deposition were reduced during winter as the  
330 meteorological conditions in the Arctic were stable and dry (Bradley et al., 1992; Bozem et al., 2019;  
331 Law and Stohl, 2007). In addition, BC emissions in EAS, EUR, and RBU regions showed obvious  
332 monthly changes with higher emissions from November to March as mentioned earlier (Section  
333 2.1.1), leading to the relatively high BC concentrations over the polar sea ice region in winter. Over  
334 the terrestrial areas within the Arctic Circle, summer BC concentrations were higher than winter,  
335 especially in Siberia and Alaska, which were attributed to intense BC emissions from biomass  
336 burning over these areas from Jun to Aug (Figure S3).

337



338 **Figure 2.** Spatial distribution of near-surface BC concentrations in (a) summer and (b) winter in the Arctic in 2010.

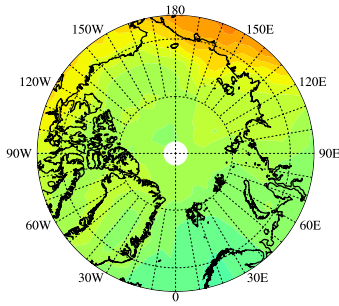
339

### 340 **3.3 Response of Arctic BC to 20% emission reductions**

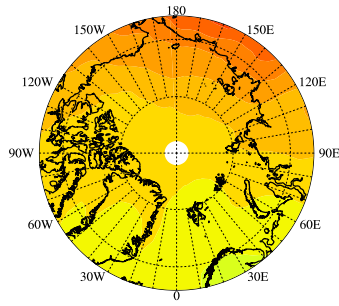
#### 341 **3.3.1 Contributions of regional emission reductions to the Arctic near-surface BC**

342 The response of the Arctic near-surface BC to 20% emission reductions from different source regions  
 343 was analyzed through emission perturbation simulations. Figure 3 shows the spatial distribution of  
 344 the referred response above in summer and in winter of 2010 based on multi-model ensemble mean  
 345 results. The source region contributions to the surface BC concentrations exhibited significant  
 346 seasonal variability with higher values in winter. The BC emission reductions in EAS almost affected  
 347 the whole Arctic, especially in winter, indicating the significance of the intercontinental transport of  
 348 BC. The spatial distribution of the Arctic near-surface BC response to SAS emission reductions was  
 349 similar to that of EAS, but the extent was much weaker. The emission reductions from EUR, NAM,  
 350 and RBU mainly affected the local and nearby areas, which was generally consistent with the spatial  
 351 pattern of emissions (Figure 1). The contribution from MDE emission reductions was very little.

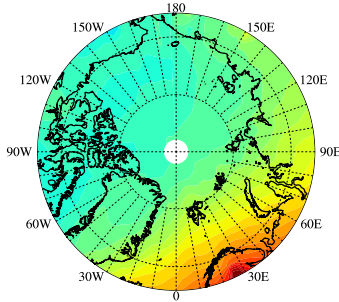
352



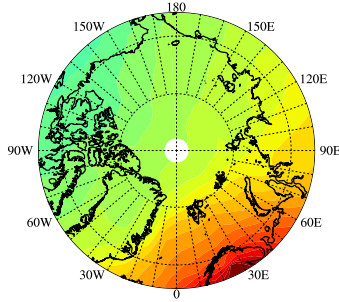
(a<sub>1</sub>) EASALL–summer



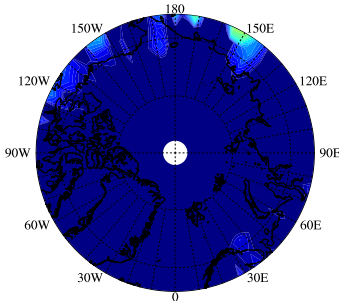
(a<sub>2</sub>) EASALL–winter



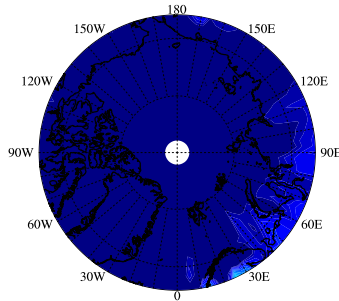
(b<sub>1</sub>) EURALL–summer



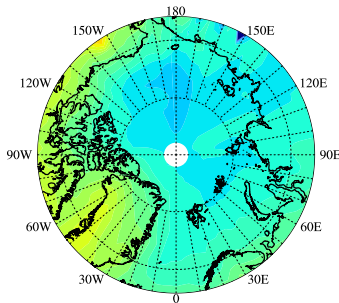
(b<sub>2</sub>) EURALL–winter



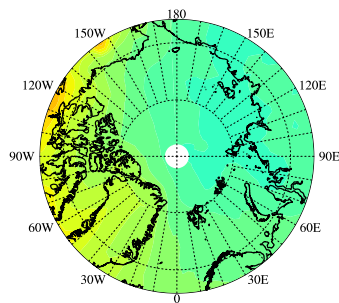
(c<sub>1</sub>) MDEALL–summer



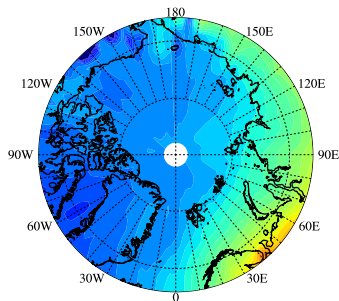
(c<sub>2</sub>) MDEALL–winter



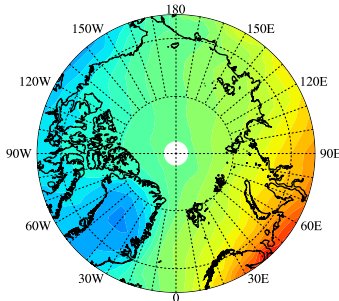
(d<sub>1</sub>) NAMALL–summer



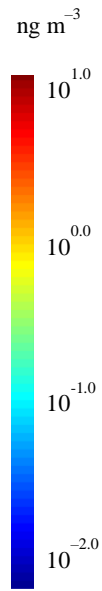
(d<sub>2</sub>) NAMALL–winter

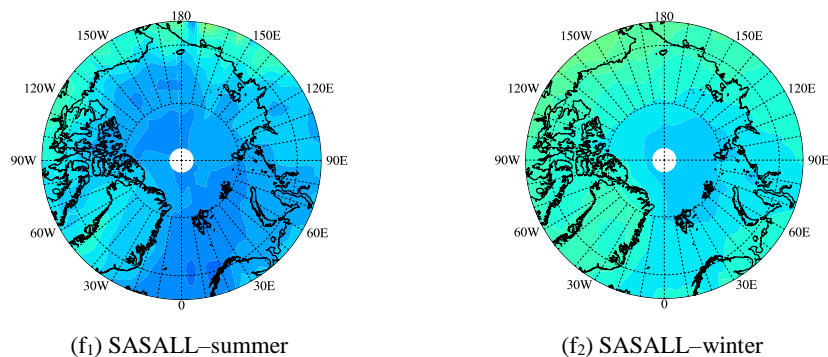


(e<sub>1</sub>) RBUALL–summer



(e<sub>2</sub>) RBUALL–winter





353 **Figure 3.** Spatial distribution of contribution of 20% emission reductions of different source regions to Arctic  
 354 near-surface BC in summer and in winter in 2010.

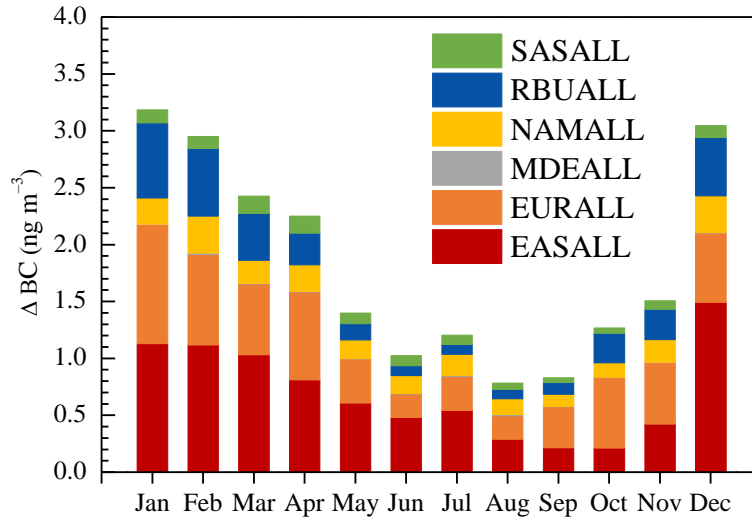
355 The monthly variations of the response of the Arctic near-surface BC concentrations to 20%  
 356 emission reductions from six source regions are presented in Figure 4. Results from the ensemble  
 357 simulations are averaged over the Arctic covering latitudinal areas from 66°N to the north pole. The  
 358 emission reductions from the total six source regions were 329.6 Gg during May to October, lower  
 359 than that of 411.9 Gg during November to April (Table 1). Correspondingly, the contributions of 20%  
 360 BC emission reductions from all six regions to Arctic monthly near-surface BC concentrations were  
 361 0.8–1.4 ng m<sup>-3</sup> during May to October and 1.5–3.2 ng m<sup>-3</sup> during November to April. Arctic  
 362 sensitivities (Arctic concentration change per unit source region emission change) for BC typically  
 363 maximized from December to February for EUR and RBU and from March to May for EAS and  
 364 NAM (Shindell et al., 2008; AMAP, 2008). The enhanced sensitivity from December to May resulted  
 365 from faster transport and slower removal during winter as the meteorological conditions in the Arctic  
 366 were stable and dry (Law and Stohl, 2007). The results of deposition changes also proved this result  
 367 well (Figure S5). The wet deposition in summer was higher than that in winter, which was 7–13  
 368 times of dry depositions. Sharma et al. (2013) found that the Arctic region (north of 70°N) was very  
 369 dry during winter with an average daily precipitation rate between 0 and 1 mm day<sup>-1</sup>. Precipitation  
 370 rates over some of the BC source regions such as Eurasia were at the same order of magnitude as the  
 371 Arctic. Less wet deposition and a shallow boundary layer resulted in higher BC concentrations near  
 372 the surface during winter. In the summertime, the Arctic region experienced 2 to 3 times higher  
 373 precipitation rates as well as wet depositions of BC relative to wintertime, thus resulting in lower  
 374 contributions to the near-surface BC concentrations.

375 The annual contribution of 20% emission reductions from EAS, EUR, MDE, NAM, RBU, and  
 376 SAS to the Arctic near-surface BC concentrations reached 0.70, 0.54, 0.01, 0.20, 0.29, and 0.09 ng



377  $\text{m}^{-3}$  in 2010, respectively, totaling about  $1.83 \text{ ng m}^{-3}$ . A simple linear interpolation suggested the  
378 contribution of 100% BC emissions from six regions to the Arctic near-surface BC concentrations  
379 was about  $9.15 \text{ ng m}^{-3}$  (five times of  $1.83 \text{ ng m}^{-3}$ ). The annual mean Arctic near-surface BC  
380 concentration from the BASE simulation was about  $18 \text{ ng m}^{-3}$  in 2010. Thus, the impact of emissions  
381 from six regions on the Arctic near-surface BC was outstanding. It should be noted that the  
382 contributions from six regions only considered anthropogenic emissions while the contribution from  
383 biomass burning was not included in the sensitivity experiments of HTAP2. It is known that  
384 wildfires in East of Russia and U.S. Alaska are important sources of BC in the Arctic region,  
385 especially in summer. Thus, the contributions from six regions to the Arctic BC should be even more  
386 dominate over the other regions by including biomass burning in RBU and NAM. The response of  
387 Arctic near-surface BC concentration was found strongest to the 20% emission reductions from EAS  
388 with the monthly contribution of  $0.2\text{--}1.5 \text{ ng m}^{-3}$ , accounting for 16.8%–49.0% of the total reduced  
389 BC concentrations resulting from all six source regions (Figure 4). On one hand, the BC emission  
390 reductions in EAS were the largest among the six source regions (Table 1). On the other hand, BC  
391 emission reductions in EAS can influence the Arctic lower troposphere via two pathways (Bozem et  
392 al., 2019; Stohl, 2006). BC from northern regions of EAS can enter into the polar dome of the Arctic  
393 in winter, as the air masses have cooled during transport. BC from eastern regions of EAS fast  
394 uplifted due to convection and then followed by high altitude transport in northerly directions.  
395 Radiative cooling eventually led to a slow descent into the polar dome area after air masses arrived  
396 in the high Arctic. It occurred both in summer and winter. In addition to EAS, BC emission reduction  
397 from EUR also showed significant impacts on the Arctic near-surface BC concentration with the  
398 monthly contribution of  $0.2\text{--}1.0 \text{ ng m}^{-3}$ , accounting for 20.1%–49.0% of the total reduced BC  
399 concentrations resulting from all six source regions (Figure 4). Among the three regions in the Arctic  
400 Circle (i.e. EUR, NAM, and RBU), EUR region had the largest BC emission reductions. Also, the  
401 relatively short distance between EUR and the Arctic made EUR the second most important source  
402 region to the Arctic. As for NAM and RBU, their 20% emission reductions induced moderate  
403 reductions of the monthly Arctic near-surface BC concentrations by  $0.1\text{--}0.3$  and  $0.1\text{--}0.7 \text{ ng m}^{-3}$ ,  
404 respectively. The contribution of 20% emission reductions from SAS to the Arctic near-surface BC  
405 concentrations was much lower of monthly contributions of  $0.0\text{--}0.2 \text{ ng m}^{-3}$  as a significant portion of  
406 BC originating from SAS accumulated in the upper troposphere (Section 3.3.2). Compared to the

407 five source regions discussed above, the response of Arctic BC concentrations to emission reductions  
408 from MDE was negligible, owing largely to the low emissions there and long distance from the  
409 Arctic.  
410



411 **Figure 4.** Monthly mean reduced concentrations of the near-surface Arctic BC due to 20% emission reductions  
412 from six source regions in 2010.

413 Figure S6 compares the contributions of 20% emission reductions to Arctic near surface BC  
414 concentrations simulated by different models. All five models showed similar monthly variations, of  
415 which CHASER\_re1 simulated high BC concentrations compared to the other models due to slow  
416 aging-speed (Sudo et al., 2015). All models showed the major source regions of Arctic BC from EAS,  
417 EUR, and RUB. NAM and SAS contributed moderately while the contribution from MDE was  
418 negligible.

419

### 420 3.3.2 Contributions of regional emission reductions to the vertical BC profiles

421 To assess the contributions from various source regions to the BC profiles based on the model  
422 ensemble mean, the vertical stratification needed to be unified as most participating models had  
423 different vertical settings. Since CHASER had a relatively coarse vertical resolution of 32 layers, the  
424 other models were unified to the same vertical stratification, as detailed in Table S2.

425 As shown in Figure 5, the contributions of regional emission reductions to BC exhibited strong  
426 vertical gradients over the Arctic. In general, the BC profiles displayed a bimodal pattern in summer,  
427 showing peaks at around 1.0–1.6 km a.s.l. (4<sup>th</sup> and 5<sup>th</sup> layers) and 8.0–8.9 km a.s.l. (13<sup>th</sup> and 14<sup>th</sup>

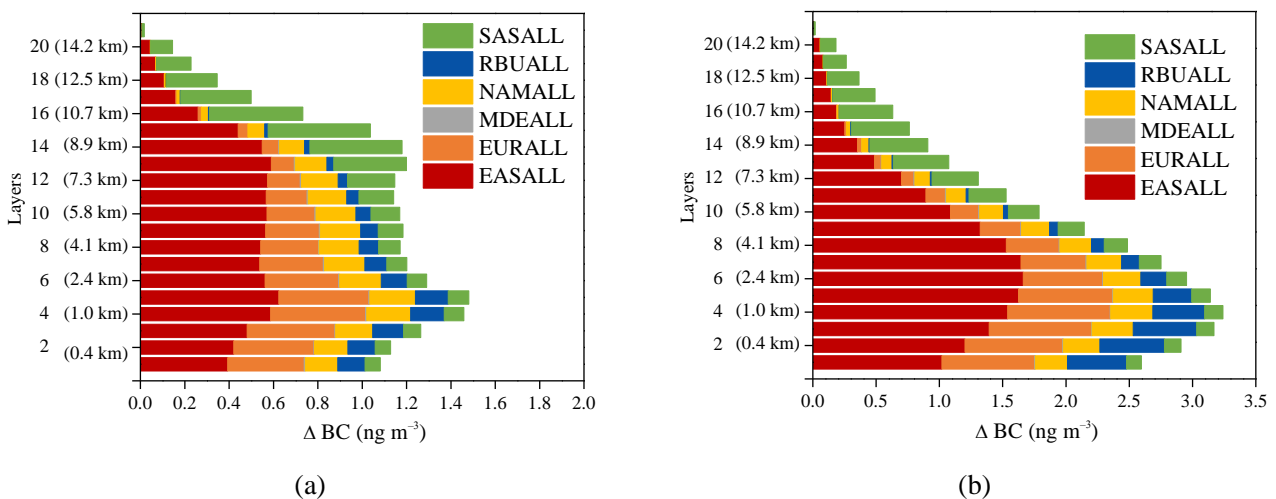
428 layers). While in winter, the BC profiles showed a unimodal pattern with peaks around 0.6–1.6 km  
429 a.s.l. (3<sup>rd</sup> – 5<sup>th</sup> layers). Long-range transport of air pollutions may occur near the planetary boundary  
430 layer (Eckhardt et al., 2003; Stohl et al., 2002). High contributions in the low layers (e.g., 3<sup>rd</sup> – 5<sup>th</sup>  
431 layers) were consistent with the height of the planetary boundary layer in the Arctic (Zhang, et al.,  
432 2018; Cheng, 2011).

433 It has been summarized that there were several major transport pathways for BC into the Arctic  
434 troposphere (Stohl, 2006). i) BC transported rapidly at low-level, followed by uplifting at the Arctic  
435 front when it is located far north. Significant deposition of BC in the Arctic occurs mostly north of  
436 70°N for this transport route. This transport route derived often from the high BC emission areas in  
437 northern EUR but seldom from the NAM and RBU. That was mainly due to that the BC emissions  
438 exist at high enough latitudes in EUR, which can be north of the polar front. However, the BC  
439 emissions in NAM and RBU were concentrated south of the polar front (Figure 1), thus BC emitted  
440 from these two regions can't be easily transported into the Arctic through this pathway. ii) Cold air  
441 masses into the polar dome transport at low-level. This pathway derived mainly from EUR and  
442 high-latitude areas of EAS during winter. The contribution of 20% emission reductions from EUR to  
443 the Arctic BC concentrations peaked at around 1.0 km a.s.l. with the multi-model ensemble mean  
444 value of 0.4 ng m<sup>-3</sup> in summer, while peaked at lower altitude of around 1.6 km a.s.l. with the value  
445 of 0.8 ng m<sup>-3</sup> in winter. iii) BC could also ascend south of the Arctic followed either by high-altitude  
446 transport or by several cycles of upward and downward transport, and finally slowly descended into  
447 the polar dome due to radiative cooling. This was the frequent transport route from source regions  
448 such as NAM, RBU, and east EAS. The contribution from NAM and RBU to the Arctic BC peaked  
449 at about 1.6 km a.s.l. (0.2 ng m<sup>-3</sup>) and 1.0 km a.s.l. (0.2 ng m<sup>-3</sup>) in summer, and peaked at about 1.0  
450 km a.s.l. (0.3 ng m<sup>-3</sup>) and 0.4 km a.s.l. (0.5 ng m<sup>-3</sup>) in winter. The contribution from EAS including  
451 pathways ii and iii, to the Arctic BC peaked at about 1.6 km a.s.l. (0.6 ng m<sup>-3</sup>) in summer and peaked  
452 at about 2.4 km a.s.l. (1.6 ng m<sup>-3</sup>) in winter. Matsui et al. (2011) pointed out that Asian  
453 anthropogenic air masses were measured most frequently in the upper troposphere, with median  
454 values of 20 ng m<sup>-3</sup> (410hPa) in April 2008 and 5 ng m<sup>-3</sup> (353hPa) in June–July 2008. In our  
455 analysis, the contribution of 20% emission from EAS and SAS to BC in the Arctic was 1.4 ng m<sup>-3</sup>  
456 (432hPa) in April 2010 and 0.7 ng m<sup>-3</sup> (375hPa) in June–July 2010. If the contribution was linearly  
457 interpolated, the contribution of 100% emission from EAS and SAS to BC in the Arctic would be

458 about  $7 \text{ ng m}^{-3}$  (432hPa) in April and  $3.5 \text{ ng m}^{-3}$  (375hPa) in June–July in 2020. In general, our  
 459 results were at the same magnitude with Matsui et al. (2011). The contribution from MDE was  
 460 negligible.

461 As shown in Figure 5, BC can also be transported into the upper troposphere of the Arctic. Air  
 462 masses preferably kept their potential temperature almost constant during transport as the  
 463 atmospheric circulation can be well described by adiabatic motions in the absence of diabatic  
 464 processes related to clouds, radiation, and turbulence. The potential temperature was low within the  
 465 polar dome area, and thus only air masses experienced diabatic cooling were able to enter the polar  
 466 dome (Stohl, 2006). That is to say, the air masses from SAS and low-latitude regions of EAS were  
 467 not easy to penetrate the polar dome but can be lifted and transported to the Arctic in the middle and  
 468 upper troposphere along the isentropes (AMAP, 2011; Barrie, 1986; Law and Stohl, 2007; Stohl,  
 469 2006). This agreed well with the previous study of Koch and Hansen (2005) and Stohl (2006). The  
 470 contribution from SAS to the Arctic BC concentrations peaked at about 9.7 km a.s.l. ( $0.4 \text{ ng m}^{-3}$ ) in  
 471 summer and 9.7 km a.s.l. ( $0.5 \text{ ng m}^{-3}$ ) winter. This was also consistent with the vertical profiles of  
 472 BC shown in Stjern et al. (2016). The polar dome boundary was variable in time and space and was  
 473 not zonally symmetric. The range of polar dome expanded southward to about  $40^\circ\text{N}$  over Eurasia in  
 474 winter as the temperature difference of different latitudes became smaller (Bozem et al., 2019; Law  
 475 and Stohl, 2007), resulting in the contribution of EAS to the Arctic BC concentrations in upper  
 476 troposphere only peak in summer at 13<sup>th</sup> layer (8.0 km a.s.l.) with the value of  $0.6 \text{ ng m}^{-3}$ .

477



478 **Figure 5.** Contribution of 20% emission reductions from six source regions to BC concentrations in different  
 479 vertical layers (a) in summer and (b) in winter in the Arctic in 2010.

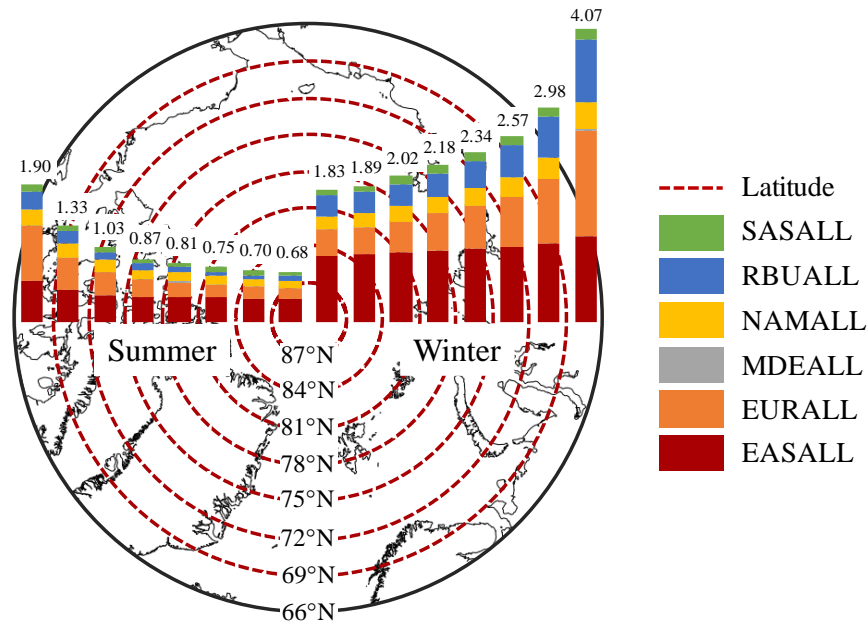
### 480 3.3.3 Contributions of emission reductions to BC in different latitudinal bands

481 To further analyze the response of the Arctic BC concentrations to emission reductions of six source  
482 regions in HTAP2, the contribution of 20% emission reductions to BC concentrations at different  
483 latitudes of the Arctic were calculated (Figures 6 and 7). In regard to the different horizontal  
484 resolution of participating models, the Arctic region (66–90°N) was divided into eight latitudinal  
485 bands with a 3-degree interval, which was based on the coarsest resolution of all models.

486 The response of the Arctic BC concentrations to emission reductions of six source regions became  
487 weaker with the increase of the latitude due to the continuous loss of BC during transport (e.g., dry  
488 and wet depositions) (Figure 6). The difference of contributions between two adjacent latitudinal  
489 bands became smaller as closer to the north pole. The contributions of 20% emission reductions to  
490 the Arctic BC concentrations near surface were the highest between 66–69°N both in summer (1.9 ng  
491 m<sup>-3</sup>) and winter (4.1 ng m<sup>-3</sup>), which were 1.4–2.8 times higher than the other latitudinal bands.

492 The contributions from EAS and EUR were higher than those from the other four regions in each  
493 latitudinal band. In detail, the contributions from EUR (0.8 ng m<sup>-3</sup> in summer and 1.5 ng m<sup>-3</sup> in  
494 winter) were higher than those from EAS (0.6 ng m<sup>-3</sup> in summer and 1.2 ng m<sup>-3</sup> in winter) in the  
495 latitudinal band of 66–69°N as the BC concentrations near surface there were more sensitive to the  
496 local emission sources. In contrast, the latitudinal contributions from EAS (0.3–0.4 ng m<sup>-3</sup> in  
497 summer and 0.9–1.1 ng m<sup>-3</sup> in winter) were higher than those from EUR (0.2–0.4 ng m<sup>-3</sup> in summer  
498 and 0.4–0.9 ng m<sup>-3</sup> in winter) in the other high latitudinal bands where long-range transport played  
499 the dominant role.

500 The downward trends of the response of the Arctic near surface BC to emission reductions with  
501 the increase of latitude from EUR and RBU were more obvious than that of other regions (Figure 6).  
502 Dry and wet depositions of BC decreased with the increase of transport distance, and the decreasing  
503 rates became slower (Figure S7). The changes of dry and wet depositions caused by emission  
504 reductions from EUR and RBU were still obvious in the Arctic region (66°N–90°N), while  
505 depositions caused by emission reductions from the other regions tended to be gentle (Figure S7).  
506 This explains why the contribution from EAS to BC at different latitudes remained almost constant  
507 while that from EUR and RBU decreased obviously from lower latitudes to the Arctic pol  
508

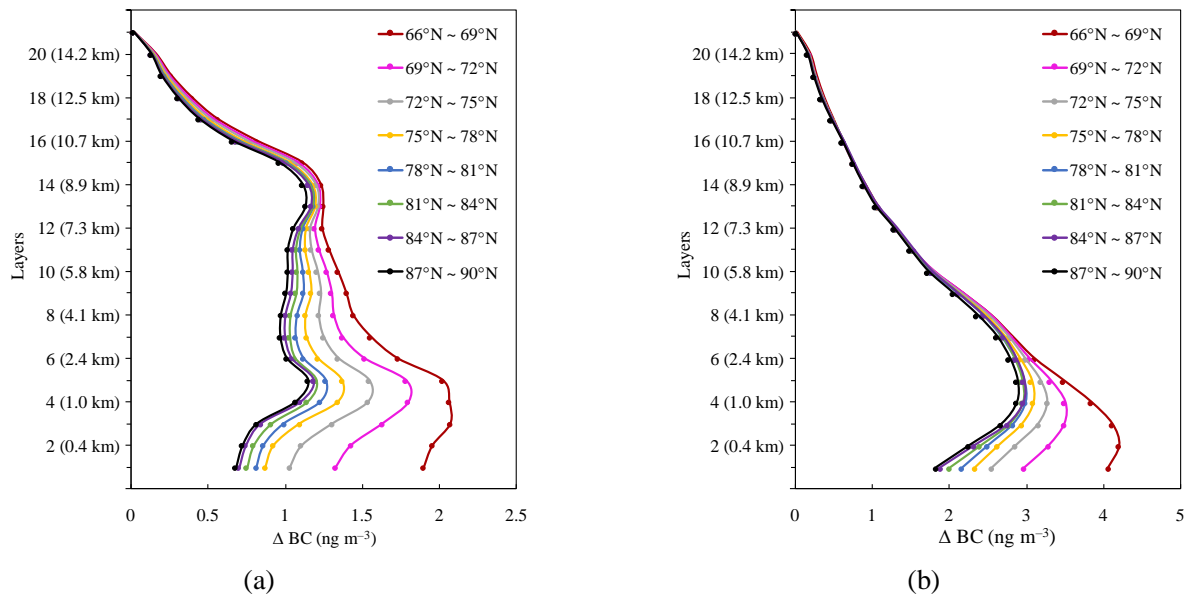


509

510 **Figure 6.** Contributions of 20% emission reductions of different regions to near-surface BC concentrations in each  
 511 latitudinal band of the Arctic. The results of summer and winter correspond to the left and right panel in the figure.

512 Figure 7 further depicts the response of the vertical Arctic BC profiles in different latitudinal bands  
 513 to 20% emission reductions. The contributions of eight latitudinal bands showed a typical bimodal  
 514 pattern in summer with peaks at 0.6–1.6 km a.s.l. (3<sup>rd</sup> – 5<sup>th</sup> layers) and 8.0–8.9 km a.s.l. (13<sup>th</sup> and 14<sup>th</sup>  
 515 layers), while the contribution displayed a single peak at the 0.4–1.0 km a.s.l. (2<sup>nd</sup> – 4<sup>th</sup> layers) in  
 516 winter. Similar to section 3.3.2, the peak value of the contribution at the low layers was due to the  
 517 transport of EAS, EUR, NAM, and RBU emission reductions to the Arctic through different  
 518 pathways both in summer and winter. The peak value in the high layers in summer was due to the  
 519 transport of EAS and SAS. However, a high contribution of 20% emission reductions to BC  
 520 concentrations in SAS was found in the high layers, while the contribution was low in other regions,  
 521 leading to a single peak in winter. The statistical results of SAS indicated that the contribution in  
 522 vertical appeared one peak at the 15<sup>th</sup> layer (9.7 km a.s.l.) with values of 0.45 and 0.48 ng m<sup>-3</sup> in  
 523 summer and winter, respectively (Figure S8).

524



525 **Figure 7.** Contributions of 20% emission reductions from all six source regions to the vertical BC concentrations of  
 526 the Arctic in different latitude bands varies with vertical layers in (a) summer and (b) winter in 2010.

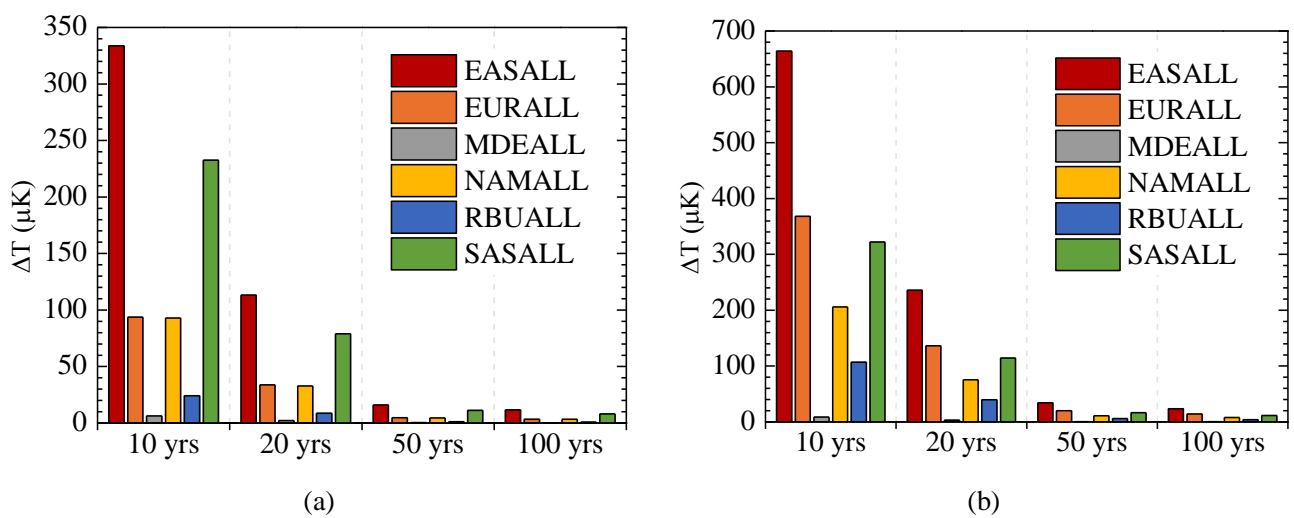
527 As same as the whole Arctic region (Section 3.3.1 & 3.3.2), the contributions of 20% emission  
 528 reductions to BC concentrations in eight latitude bands were higher in winter than in summer,  
 529 whether near surface or in vertical. The contribution of 20% emission reductions from all six source  
 530 regions to BC concentrations in eight latitude bands of the Arctic near surface was 0.7–1.9 ng m<sup>-3</sup> in  
 531 summer and 1.8–4.1 ng m<sup>-3</sup> in winter, respectively (Figure 6). The high BC peak at around 0.6–1.6  
 532 km a.s.l. (3<sup>rd</sup> – 5<sup>th</sup> layers) was 1.1–2.1 ng m<sup>-3</sup> in summer, and 2.9–4.2 ng m<sup>-3</sup> in winter (Figure 7).

### 533 3.4 Benefit of BC emission reductions on the decrease of Arctic temperature

534 The impact of BC emission reductions on decreasing the Arctic (60–90°N) surface temperature was  
 535 assessed by using ARTP (See methods in Section 2.2). Aerosol effects, BC deposition on snow, and  
 536 BC semi-direct were considered in the calculation of ARTP (Aamaas et al., 2017). As shown in  
 537 Figure 8, the response of Arctic surface temperature to emission reductions was the most significant  
 538 at the time scale of 10 years and then gradually decreased with the passage of time. For each source  
 539 region, the Arctic temperature response was significantly higher in winter than in summer as ARTP  
 540 was seasonal dependent with higher values in the colder seasons. Obviously, the Arctic surface  
 541 temperature benefited the most from BC emission reductions from EAS with more than 300 and 660  
 542 μK decreases in summer and winter after 10 years, respectively. The influences of EUR and NAM  
 543 emission reductions on the temperature decrease were similar in summer, reaching about 3–90 μK

544 after 10, 20, 50, and 100 years. However, in winter, the influence of emission reductions from NAM  
 545 on temperature decrease (8–200  $\mu\text{K}$ ) was weaker than that from EUR (14–370  $\mu\text{K}$ ). This was mainly  
 546 due to the difference of ARTPs between EUR and NAM was not obvious compared with the  
 547 difference of emission reductions from NAM and EUR in summer and winter. The responses of the  
 548 temperature decrease to emission reductions from RBU were 9–20  $\mu\text{K}$  in summer and 4–100  $\mu\text{K}$  in  
 549 winter after 10-100years, respectively, which were smaller than that from EUR and NAM. This can  
 550 be explained by the low BC emission reductions from RBU (Table 1). The response of the  
 551 temperature decrease to emission reductions from SAS in winter (10–320  $\mu\text{K}$ ) was similar to that  
 552 from EUR, while this response in summer (8–230  $\mu\text{K}$ ) was more than twice that of EUR. Although  
 553 the ARTP of EUR was higher than that of SAS, the BC emission reductions from SAS were much  
 554 higher than that from EUR and the difference between emission reductions from the two regions was  
 555 more obvious in summer (Table 1). In spite of the higher Arctic temperature response to EAS than  
 556 SAS in the target year of this study, a number of studies have shown that BC emissions in South Asia  
 557 were increasing in recent years (Sahu et al., 2008; Paliwal et al., 2016; Sharma et al., 2019) while the  
 558 emissions of East Asia were exhibiting a downward trend especially from China (Chen et. al., 2016),  
 559 thus it should be given more attention to the impact assessment of South Asia on the Arctic in the  
 560 future. The minimum temperature response was found from MDE due to the least emission  
 561 reductions and small ARTP.

562

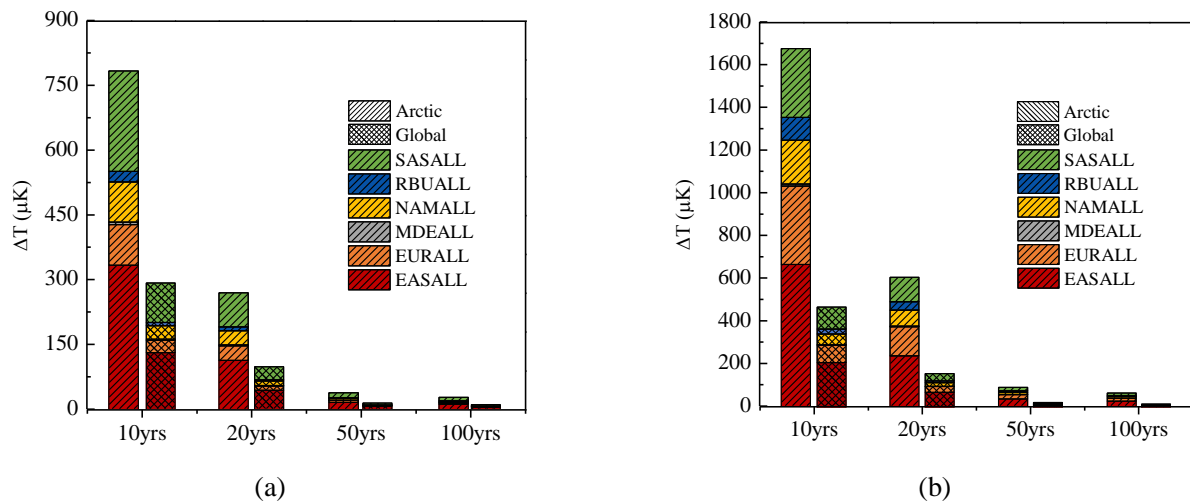


563 **Figure 8.** Arctic surface temperature response to 20% regional BC emission reductions in (a) summer and (b)  
 564 winter after 10, 20, 50, and 100 years.

565 In addition, the impacts of BC emission reductions from six source regions on the Arctic and



566 global surface temperature were compared in this study (Figure 9). Due to the BC emission  
 567 reductions from the six source regions, the surface temperature in the Arctic decreased 27–780  $\mu\text{K}$  in  
 568 summer and 61–1675  $\mu\text{K}$  in winter after 10, 20, 50, and 100 years, which were higher than that of  
 569 the global with the values of 10–290  $\mu\text{K}$  in summer and 16–470  $\mu\text{K}$  in winter. It can be seen that the  
 570 difference of the temperature response between the Arctic and the globe was more obvious in winter.  
 571 Overall, the response of the Arctic surface temperature was more sensitive to emissions perturbation  
 572 than that of the globe surface temperature.  
 573



574 **Figure 9.** Global and Arctic surface temperature responses to 20% regional BC emission reductions in (a) summer  
 575 and (b) winter after 10, 20, 50, and 100 years.

576 It should be noted the estimation of temperature response was subject to large uncertainties for the  
 577 following reasons. On the one hand, even though the HTAP2 emissions database were all constructed  
 578 by bottom-up methods, the different inventories and spatiotemporal distributions were constructed  
 579 with sub-regional (country, state, county or province level) activity data and emission factors, which  
 580 lead to inconsistencies at the borders between two adjacent inventories. The version 5 of Evaluating  
 581 the Climate and Air Quality Impacts of Short-Lived Pollutants (ECLIPSEv5, <http://eclipse.nilu.no>)  
 582 estimated a 2010 emission inventory, that serves also as a reference point for all projections  
 583 (Janssens-Maenhout et al., 2015). At the global level, a relatively good agreement was found with  
 584 small relative emission differences compared with the ECLIPSEv5 emission inventory for the  
 585 aggregated sectors in 2010. However, larger differences of 29% between HTAP2 and ECLIPSEv5  
 586 emissions was present for BC since ECLIPSEv5 relied on provincial statistics for China which  
 587 resulted from higher coal consumption than reported national statistics. Hoesly et al. (2018) provided

588 a sectoral and gridded historical (1750–2014) anthropogenic emission inventory for use in the  
589 Coupled Model Intercomparison Project phase 6 (CMIP6). The amount of global BC anthropogenic  
590 emissions was 7.7 Tg/year in 2010 from the CMIP6 emissions, which was larger than that from  
591 HTAP2 emissions (5.5 Tg/year). This was mainly due to the energy, transportation, and international  
592 shipping sectors of CMIP6 were higher than those of HTAP2.

593 On the other hand, the time evolution of  $R_T$ , a parameter in the calculation of ARTP was also one  
594 factor causing the uncertainty of temperature response calculation. This impulse response function  
595 was only based on one coupled atmosphere-ocean climate model GISS-ER in this study, while Olivie  
596 and Peters (2013) have found a spread in the GTP (20) value of BC of about  $-60$  to  $+80\%$  due to  
597 variability of  $R_T$  among various models. However, the uncertainty in  $R_T$  was less relevant for the  
598 regional patterns. Forcing-response coefficients didn't exist on a seasonal basis since emissions  
599 occurring during Northern Hemisphere summer and winter season were differentiated (Aamaas et al,  
600 2017). Hence, the seasonal differences presented here in the ARTP values were not due to potential  
601 differences in the response sensitivities, but due to differences in the RF. The temperature response  
602 will vary by species and location, such as between land surface and ocean surface. These differences  
603 are not accounted for in this study, but the increased efficacy in the RCS matrix towards the NH can  
604 be partly attributed to a larger land area fraction in the NH (Shindell et al., 2015). Besides, recent  
605 studies have found that the positive radiation budget of BC being largely compensated for by rapid  
606 atmospheric adjustment, this means that the responses of surface temperatures to BC tends to be  
607 weaker than expected (Stjern et al., 2017; Takemura and Suzuki, 2019).

608 Although the HTAP2 emissions database contain uncertainties and ARTP calculations are  
609 simplifications, these emission metrics are useful, simple, and quick approximations for calculating  
610 the temperature response in the different latitude bands for emissions of BC. It should be noted that  
611 the estimated responses of Arctic surface temperature to 20% emission reductions were only valid for  
612 the comparison among different source regions but cannot be used to reflect the actual change of  
613 temperature. On the one hand, in reality, not all emissions sectors of a specific source region cannot  
614 be reduced by 20% at the same time. On the other hand, there were many other factors (e.g.  
615 greenhouse gases, sea ice coverage) that can affect the temperature change in the Arctic besides BC.

## 616 4. Conclusions

617 The CAMchem, CHASER\_re1, GEOS-Chem, GOCART, and Oslo CTM3 in HTAP2 experiment  
618 were used in this study to estimate the responses of Arctic BC to multi-region emission reductions in  
619 2010. Six regions (e.g., EAS, EUR, MDE, RBU, NAM, and SAS) were selected as the source  
620 regions and the Arctic was the receptor region. HTAP2 set up the base scenario with all BC  
621 emissions, and also simulated BC concentrations with 20% reduction of anthropogenic emissions.  
622 The AGPT was further used to calculate the benefit of BC emission reductions on the decrease of  
623 Arctic temperature.

624 The statistical results of 20% BC emission reductions showed that emission reductions in EAS  
625 were the largest with the values of 355.6 Gg yr<sup>-1</sup>, followed by SAS (232.5 Gg yr<sup>-1</sup>), EUR (65.3 Gg  
626 yr<sup>-1</sup>), NAM (62.2 Gg yr<sup>-1</sup>), RBU (18.6 Gg yr<sup>-1</sup>), and MDE (5.3 Gg yr<sup>-1</sup>). The BC emission  
627 reductions in the EAS, EUR, and RBU were higher from November to March.

628 The temporal variations of simulations from different models were relatively consistent as the  
629 correlations of the simulated BC concentrations among different models ranged from 0.33 to 0.98.  
630 However, the simulated BC concentrations didn't agree so well with observations at monitoring sites  
631 except Zeppelin. In order to reduce the difference of simulation performance of each model in  
632 different areas of the Arctic, the model ensemble mean was used for analysis.

633 The contribution of 20% BC emission reductions from EAS, EUR, MDE, NAM, RBU, and SAS  
634 to the Arctic near-surface BC concentrations reached 0.70, 0.54, 0.01, 0.20, 0.29, and 0.09 ng m<sup>-3</sup>,  
635 respectively. Correspondingly, the reduced column BC loadings from the six regions above over the  
636 Arctic was 8521.7, 2789.1, 28.8, 1762.1, 998.6, and 3640.2 ng m<sup>-2</sup>, respectively.

637 The response of Arctic near-surface BC concentrations to 20% emission reductions from EAS and  
638 EUR was larger than other four source regions, with the monthly value of 0.2–1.5 ng m<sup>-3</sup> and 0.2–1.0  
639 ng m<sup>-3</sup>, accounting for 16.8%–49.0% and 20.1%–49.0% of the total contributions from all six  
640 regions, respectively. The BC profiles displayed a bimodal pattern in summer with peaks at around  
641 1.0–1.6 km a.s.l. (4<sup>th</sup> and 5<sup>th</sup> layers) and 8.0–8.9 km a.s.l. (13<sup>th</sup> and 14<sup>th</sup> layers). While the BC profiles  
642 showed a unimodal pattern with peaks around 0.6–1.6 km a.s.l. (3<sup>rd</sup> – 5<sup>th</sup> layers) in winter.

643 The response of Arctic BC to emission reductions from source regions in winter was higher than

644 that in summer. The contributions of 20% emission reductions to the Arctic BC concentrations near  
645 surface were the highest between 66–69°N both in summer (1.9 ng m<sup>-3</sup>) and winter (4.1 ng m<sup>-3</sup>), and  
646 became weaker with the increase of the latitude.

647 The response of Arctic temperature to BC emission reductions was the most significant at the time  
648 scale of 10 years and then gradually decreased with the passage of time. The Arctic had benefited the  
649 most from emission reduction in EAS with more than 300 and 660 μK decreases in summer and  
650 winter after 10 years, respectively. The Arctic temperature response was more sensitive to the whole  
651 globe in regard of the same emissions perturbation. The estimation of temperature response was  
652 subject to large uncertainties due to the uncertainties in the calculation of ARTP and emissions of BC  
653 in source regions.

654 Overall, this study provided insights on the source regions and seasonal contributions of Arctic BC  
655 from the most recent international ensemble modeling efforts. The discrepancy between model  
656 results and observations and the spread among different HTAP models may be attributed to various  
657 factors such as emissions in the remote Arctic, physical parameterizations, and convection and  
658 deposition processes. This would subsequently result in large uncertainties of the climatic effects of  
659 air pollutants. More observation sites on the typical transport pathways from sources regions to the  
660 Arctic should be planned to improve the model capability of simulating the transport behavior of  
661 black carbon.

## 662 **Data availability**

663 All data used in this paper can be obtained through the AeroCom servers and web interfaces,  
664 accessible at <http://aerocom.met.no>.

665

## 666 **Author contributions**

667 KH and JSF designed this study. ML, KS, DH, TK, MC, and ST performed modeling. NZ analyzed  
668 data and wrote the paper. All have commented on and reviewed the paper.

669

670 **Competing interests.**

671 The authors declare that they have no conflict of interest.

672

673 **Acknowledgements**

674 We sincerely thank for the HTAPv2 international initiative. This work was partially supported by  
675 the National Key R&D Program of China (2018YFC0213105), the National Natural Science  
676 Foundation of Shanghai (18230722600), and the National Natural Science Foundation of China  
677 (91644105).

678

679 **References**

- 680 Aamaas, B., Berntsen, T. K., Fuglestedt, J. S., Shine, K. P., and Bellouin, N.: Regional emission metrics for  
681 short-lived climate forcers from multiple models, *Atmos. Chem. Phys.*, 16, 7451–7468,  
682 <https://doi.org/10.5194/acp-16-7451-2016>, 2016.
- 683 Aamaas, B., Berntsen, T. K., Fuglestedt, J. S., Shine, K. P., and Collins, W. J.: Regional temperature change  
684 potentials for short-lived climate forcers based on radiative forcing from multiple models, *Atmos. Chem. Phys.*,  
685 17, 10795-10809, 10.5194/acp-17-10795-2017, 2017.
- 686 AMAP: Black carbon and ozone as Arctic climate forcers. Arctic Monitoring and Assessment Programme (AMAP),  
687 Oslo, Norway. vii + 116 pp, 2015.
- 688 AMAP: Snow, Water, Ice and Permafrost in the Arctic (SWIPA) 2017. Arctic Monitoring and Assessment  
689 Programme (AMAP), Oslo, Norway. xiv + 269 pp. ISBN 978–82–7971–101–8, 2017.
- 690 AMAP: The Impact of Black Carbon on Arctic Climate. By: Quinn, P. K., Stohl, A., Arneth, A., Berntsen, T.,  
691 Burkhardt, J. F., Christensen, J., Flanner, M., Kupiainen, K., Lihavainen, H., Shepherd, M., Shevchenko, V.,  
692 Skov, H., and Vestreng., V., Arctic Monitoring and Assessment Programme (AMAP), Oslo. 72 pp, 2011.
- 693 AMAP: The Impact of Short-Lived Pollutants on Arctic Climate. By: Quinn, P. K., Bates, T. S., Baum, E., Bond, T.,  
694 Burkhardt, J. F., Fiore, A. M., Flanner, M. G., Garrett, T., Koch, D., McConnell, J. R., Shindell, D., and Stohl, A.,  
695 Arctic Monitoring and Assessment Programme (AMAP), Oslo, Norway, 2008.
- 696 Barrie, L. A.: Arctic air pollution: an overview of current knowl- edge, *Atmos. Environ.*, 20, 643–663, 1986.
- 697 Bond, T. C., Doherty, S. J., Fahey, D. W., Forster, P. M., Berntsen, T., DeAngelo, B. J., Flanner, M. G., Ghan, S.,  
698 Kärcher, B., Koch, D., Kinne, S., Kondo, Y., Quinn, P. K., Sarofim, M. C., Schultz, M. G., Schulz, M.,  
699 Venkataraman, C., Zhang, H., Zhang, S., Bellouin, N., Guttikunda, S. K., Hopke, P. K., Jacobson, M. Z.,  
700 Kaiser, J. W., Klimont, Z., Lohmann, U., Schwarz, J. P., Shindell, D., Storelvmo, T., Warren, S. G., and Zender,  
701 C. S.: Bounding the role of black carbon in the climate system: A scientific assessment, *J. Geophys.*  
702 *Res.–Atmos.*, 118, 5380–5552, <https://doi.org/10.1002/jgrd.50171>, 2013.
- 703 Bozem, H., Hoor, P., Kunkel, D., Köllner, F., Schneider, J., Herber, A., Schulz, H., Leaitch, W. R., Aliabadi, A. A.,  
704 Willis, M. D., Burkart, J., and Abbatt, J. P. D.: Characterization of transport regimes and the polar dome during  
705 Arctic spring and summer using in situ aircraft measurements, *Atmos. Chem. Phys.*, 19, 15049-15071,  
706 10.5194/acp-19-15049-2019, 2019.
- 707 Bradley, R. S., Keimig, F. T., and Diaz, H. F.: Climatology of surface-based inversions in the North American  
708 Arctic, *J. Geophys. Res.*, 97, 15 699, <https://doi.org/10.1029/92JD01451>, 1992.
- 709 Chen, D. S., Zhao, Y. H., Nelson, P., Li, Y., Wang, X. T., Zhou, Y., Lang, J. L., and Guo, X. R.: Estimating ship  
710 emissions based on AIS data for port of Tianjin, China. *Atmos. Environ.* 145: 10–18.  
711 <http://dx.doi.org/10.1016/j.atmosenv.2016>.
- 712 Cheng, G: Analysis of observational data of atmospheric boundary layer characteristics in the Arctic (in Chinese),  
713 Nanjing University of information engineering. 2011.
- 714 Chin, M., Rood, R. B., Lin, S.-J., Müller, J.-F., and Thompson, A. M.: Atmospheric sulfur cycle simulated in the  
715 global model GOCART: Model description and global properties, *J. Geophys. Res.–Atmos.*, 105,  
716 24671–24687, doi:10.1029/2000JD900384, 2000.
- 717 Clarke, A. D. and Noone, K. J.: Soot in the Arctic snowpack: a cause for perturbations in radiative transfer, *Atmos.*  
718 *Environ.*, 19, 2045–2053, [https://doi.org/10.1016/0004-6981\(85\)90113-1](https://doi.org/10.1016/0004-6981(85)90113-1), 1985.
- 719 Collins, W. J., Fry, M. M., Yu, H., Fuglestedt, J. S., Shindell, D. T., and West, J. J.: Global and regional

720 temperature-change potentials for near-term climate forcers, *Atmos. Chem. Phys.*, 13, 2471–2485,  
721 10.5194/acp-13-2471-2013, 2013.

722 Eckhardt, S., Stohl, A., Beirle, S., Spichtinger, N., James, P., Forster, C., Junker, C., Wagner, T., Platt, U., and  
723 Jennings, S. G.: The North Atlantic Oscillation controls air pollution transport to the Arctic, *Atmos. Chem.*  
724 *Phys.*, 3, 1769–1778, <https://doi.org/10.5194/acp-3-1769-2003>, 2003.

725 Flanner, M. G.: Arctic climate sensitivity to local black carbon, *J. Geophys. Res.-Atmos.*, 118, 1840–1851,  
726 <https://doi.org/10.1002/jgrd.50176>, 2013.

727 Fuglestedt, J. S., Shine, K. P., Berntsen, T., Cook, J., Lee, D. S., Stenke, A., Skeie, R. B., Velders, G. J. M., and  
728 Waitz, I. A.: Transport impacts on atmosphere and climate: metrics, *Atmos. Environ.*, 44, 4648–4677,  
729 <https://doi.org/10.1016/j.atmosenv.2009.04.044>, 2010.

730 Galmarini, S., Koffi, B., Solazzo, E., Keating, T., Hogrefe, C., Schulz, M., Benedictow, A., Griesfeller, J. J.,  
731 Janssens-Maenhout, G., Carmichael, G., Fu, J., and Dentener, F.: Technical note: Coordination and  
732 harmonization of the multi-scale, multi-model activities HTAP2, AQMEII3, and MICS-Asia3: simulations,  
733 emission inventories, boundary conditions, and model output formats, *Atmos. Chem. Phys.*, 17, 1543–1555,  
734 2017.

735 Garrett, T. J. and Zhao, C.: Increased Arctic cloud longwave emissivity associated with pollution from mid-latitudes,  
736 *Nature*, 440, 787–789, 2006.

737 Hansen, J. and Nazarenko, L.: Soot climate forcing via snow and ice albedos, *P. Natl Acad. Sci. USA*, 101,  
738 423–428, <https://doi.org/10.1073/pnas.2237157100>, 2004.

739 Henze, D. K., Hakami, A., and Seinfeld, J. H.: Development of the adjoint of GEOS–Chem, *Atmos. Chem. Phys.*, 7,  
740 2413–2433, [doi:10.5194/acp-7-2413-2007](https://doi.org/10.5194/acp-7-2413-2007), 2007.

741 Hoesly R. M., Smith S. J., Feng L. Y., Klimont Z., Janssens-Maenhout G., Pitkanen T., Seibert J. J., Vu L., Andres R.  
742 J., Bolt R. M., Bond T. C., Dawidowski L., Kholod N., Kurokawa J., Li M., Liu L., Lu Z. F., Moura M. C. P.,  
743 O’Rourke P. R., Zhang Q.: Historical (1750–2014) anthropogenic emissions of reactive gases and aerosols  
744 from the Community Emissions Data System (CEDS), *Geosci. Model Dev.*, 11, 369–408,  
745 10.5194/gmd-11-369-2018, 2018.

746 Hogrefe, C., Liu, P., Pouliot, G., Mathur, R., Roselle, S., Flemming, J., Lin, M., and Park, R. J.: Impacts of different  
747 characterizations of large-scale background on simulated regional-scale ozone over the continental United  
748 States, *Atmos. Chem. Phys.*, 18, 3839–3864, 2018.

749 Huang, K., Fu, J. S., Hodson, E. L., Dong, X., Cresko, J., Prikhodko, V. Y., Storey, J. M., and Cheng, M.-D.:  
750 Identification of missing anthropogenic emission sources in Russia: Implication for modeling Arctic haze,  
751 *Aerosol Air Qual. Res.*, 14, 1799–1811, 2014.

752 Huang, K., Fu, J. S., Prikhodko, V. Y., Storey, J. M., Romanov, A., Hodson, E. L., Cresko, J., Morozova, I., Ig-  
753 natieva, Y., and Cabaniss, J.: Russian anthropogenic black carbon: Emission reconstruction and Arctic black  
754 carbon simulation, *J. Geophys. Res.-Atmos.*, 120, 11306–11333, <https://doi.org/10.1002/2015JD023358>, 2015.

755 IPCC: Climate Change: The Intergovernmental Panel on Climate Change Scientific Assessment. The  
756 Intergovernmental Panel on Climate Change (IPCC), Cambridge University Press, Cambridge, UK, 1990.

757 IPCC: Climate Change 2001: The Scientific Basis. Intergovernmental Panel on Climate Change. The  
758 Intergovernmental Panel on Climate Change (IPCC), Cambridge University Press, Cambridge, UK, 2001.

759 Janssens-Maenhout, G., Crippa, M., Guizzardi, D., Dentener, F., Muntean, M., Pouliot, G., Keating, T., Zhang, Q.,  
760 Kurokawa, J., Wankmüller, R., Denier van der Gon, H., Kuenen, J. J. P., Klimont, Z., Frost, G., Darras, S.,  
761 Koffi, B., and Li, M.: HTAP\_v2.2: a mosaic of regional and global emission grid maps for 2008 and 2010 to  
762 study hemispheric transport of air pollution, *Atmos. Chem. Phys.*, 15, 11411–11432,  
763 10.5194/acp-15-11411-2015, 2015.

764 Jonson, J. E., Schulz, M., Emmons, L., Flemming, J., Henze, D., Sudo, K., Tronstad Lund, M., Lin, M., Benedictow,

765 A., Koffi, B., Dentener, F., Keating, T., Kivi, R., and Davila, Y.: The effects of intercontinental emission  
766 sources on European air pollution levels, *Atmos. Chem. Phys.*, 18, 13655–13672, 2018.

767 Koch, D. and Hansen, J.: Distant origins of Arctic black carbon: A Goddard Institute for Space Studies ModelE  
768 experiment, *J. Geophys. Res.–Atmos.*, 110, D04204, <https://doi.org/10.1029/2004JD005296>, 2005.

769 Lamarque, J. F., Emmons, L. K., Hess, P. G., Kinnison, D. E., Tilmes, S., Vitt, F., Heald, C. L., Holland, E. A.,  
770 Lauritzen, P. H., Neu, J., Orlando, J. J., Rasch, P. J., and Tyndall, G. K.: CAM-chem: description and  
771 evaluation of interactive atmospheric chemistry in the Community Earth System Model, *Geosci. Model Dev.*,  
772 5, 369–411, [10.5194/gmd-5-369-2012](https://doi.org/10.5194/gmd-5-369-2012), 2012.

773 Law, K. S. and Stohl, A.: Arctic air pollution: origins and impacts, *Science*, 315, 1537–1540,  
774 <https://doi.org/10.1126/science.1137695>, 2007.

775 Liang, C.-K., West, J. J., Silva, R. A., Bian, H., Chin, M., Davila, Y., Dentener, F. J., Emmons, L., Flemming, J.,  
776 Folberth, G., Henze, D., Im, U., Jonson, J. E., Keating, T. J., Kucsera, T., Lenzen, A., Lin, M., Lund, M. T., Pan,  
777 X., Park, R. J., Pierce, R. B., Sekiya, T., Sudo, K., and Takemura, T.: HTAP2 multi-model estimates of  
778 premature human mortality due to intercontinental transport of air pollution and emission sectors, *Atmos.*  
779 *Chem. Phys.*, 18, 10497–10520, 2018.

780 Lund, M. T., Berntsen, T. K., Heyes, C., Klimont, Z., and Samset, B. H.: Global and regional climate impacts of  
781 black carbon and co-emitted species from the on-road diesel sector, *Atmos. Environ.*, 98, 50–58,  
782 <https://doi.org/10.1016/j.atmosenv.2014.08.033>, 2014.

783 Lund, M. T., Aamaas, B., Berntsen, T., Bock, L., Burkhardt, U., Fuglestad, J. S., and Shine, K. P.: Emission  
784 metrics for quantifying regional climate impacts of aviation, *Earth Syst. Dynam.*, 8, 547–563,  
785 <https://doi.org/10.5194/esd-8-547-2017>, 2017.

786 Lund, M. T., Myhre, G., Haslerud, A. S., Skeie, R. B., Griesfeller, J., Platt, S. M., Kumar, R., Myhre, C. L., and  
787 Schulz, M.: Concentrations and radiative forcing of anthropogenic aerosols from 1750 to 2014 simulated with  
788 the Oslo CTM3 and CEDS emission inventory, *Geosci. Model Dev.*, 11, 4909–4931,  
789 <https://doi.org/10.5194/gmd-11-4909-2018>, 2018.

790 Marelle, L., Thomas, J. L., Raut, J.-C., Law, K. S., Jalkanen, J.-P., Johansson, L., Roiger, A., Schlager, H., Kim, J.,  
791 Reiter, A., and Weinzierl, B.: Air quality and radiative impacts of Arctic shipping emissions in the summertime  
792 in northern Norway: from the local to the regional scale, *Atmos. Chem. Phys.*, 16, 2359–2379,  
793 <https://doi.org/10.5194/acp-16-2359-2016>, 2016.

794 Matsui, H., Kondo, Y., Moteki, N., Takegawa, N., Sahu, L. K., Zhao, Y., Fuelberg, H. E., Sessions, W. R., Diskin, G.,  
795 Blake, D. R., Wisthaler, A., Koike, M.: Seasonal variation of the transport of black carbon aerosol from the  
796 Asian continent to the Arctic during the ARCTAS aircraft campaign, *J. Geophys. Res.–Atmos.*, 116, D05202,  
797 [doi:10.1029/2010JD015067](https://doi.org/10.1029/2010JD015067).

798 Miao, Y. C., Guo, J. P., Liu, S. H., Liu, H., Zhang, G., Yan, Y., He, J.: Relay transport of aerosols to  
799 Beijing–Tianjin–Hebei region by multiscale atmospheric circulations, *Atmos. Environ.*, 165, 35–45,  
800 <https://doi.org/10.1016/j.atmosenv.2017.06.032>, 2017.

801 Myhre, G., Shindell, D., Breon, F.-M., Collins, W., Fuglestad, J., Huang, J., Koch, D., Lamarque, J.-F., Lee, D.,  
802 Mendoza, B., Nakajima, T., Robock, A., Stephens, G., Takemura, T., and Zhang, H.: Anthropogenic and  
803 Natural Radiative Forcing, in: *Climate Change 2013: The Physical Science Basis. Contribution of Working*  
804 *Group I to the Fifth Assessment Report of the Intergovernmental Panel on Climate Change*, edited by:  
805 Stocker, T. F., Qin, D., Plattner, G.-K., Tignor, M., Allen, S. K., Boschung, J., Nauels, A., Xia, Y., Bex, V., and  
806 Midgley, P. M., Cambridge University Press, Cambridge, UK and New York, NY, USA, 2013.

807 Olivié, D. J. L. and Peters, G. P.: Variation in emission metrics due to variation in CO<sub>2</sub> and temperature impulse  
808 response functions, *Earth Syst. Dynam.*, 4, 267–286, <https://doi.org/10.5194/esd-4-267-2013>, 2013.

809 Paliwal, U., Sharma, M., and Burkhardt, J. F.: Monthly and spatially resolved black carbon emission inventory of



810 India: uncertainty analysis, *Atmos. Chem. Phys.*, 16, 12457–12476, 10.5194/acp-16-12457-2016, 2016.

811 Sahu, S. K., Beig, G., and Sharma, C.: Decadal growth of black carbon emissions in India, *Geophysical Research*  
812 *Letters*, 35, 10.1029/2007gl032333, 2008.

813 Samset, B. H., Myhre, G., Schulz, M., Balkanski, Y., Bauer, S., Bernsten, T. K., Bian, H., Bellouin, N., Diehl, T.,  
814 Easter, R. C., Ghan, S. J., Iversen, T., Kinne, S., Kirkevåg, A., Lamarque, J. F., Lin, G., Liu, X., Penner, J. E.,  
815 Seland, Ø., Skeie, R. B., Stier, P., Takemura, T., Tsigaridis, K., and Zhang, K.: Black carbon vertical profiles  
816 strongly affect its radiative forcing uncertainty, *Atmos. Chem. Phys.*, 13, 2423–2434,  
817 10.5194/acp-13-2423-2013, 2013.

818 Sand, M., Bernsten, T. K., von Salzen, K., Flanner, M. G., Langner, J., and Victor, D. G.: Response of Arctic  
819 temperature to changes in emissions of short-lived climate forcers, *Nature Clim. Change*, 6, 286–289,  
820 10.1038/nclimate2880, 2016.

821 Sekiya, T., Miyazaki, K., Ogochi, K., Sudo, K., and Takigawa, M.: Global high-resolution simulations of  
822 tropospheric nitrogen dioxide using CHASER V4.0, *Geosci. Model Dev.*, 11, 959–988,  
823 10.5194/gmd-11-959-2018, 2018.

824 Sharma, S., Ishizawa, M., Chan, D., Lavoué, D., Andrews, E., Eleftheriadis, K., and Maksyutov, S.: 16-year  
825 simulation of Arctic black carbon: Transport, source contribution, and sensitivity analysis on deposition,  
826 *Journal of Geophysical Research: Atmospheres*, 118, 943–964, 10.1029/2012jd017774, 2013.

827 Sharma, G., Sinha, B., Pallavi, Hakkim, H., Chandra, B. P., Kumar, A., and Sinha, V.: Gridded Emissions of CO,  
828 NO<sub>x</sub>, SO<sub>2</sub>, CO<sub>2</sub>, NH<sub>3</sub>, HCl, CH<sub>4</sub>, PM<sub>2.5</sub>, PM<sub>10</sub>, BC, and NMVOC from Open Municipal Waste Burning in  
829 India, *Environ Sci Technol*, 53, 4765–4774, 10.1021/acs.est.8b07076, 2019.

830 Shine, K. P., Fuglestedt, J. S., Hailemariam, K., and Stuber, N.: Alternatives to the Global Warming Potential for  
831 Comparing Climate Impacts of Emissions of Greenhouse Gases, *Climatic Change*, 68, 281–302,  
832 10.1007/s10584-005-1146-9, 2005

833 Shindell, D. and Faluvegi, G.: Climate response to regional radiative forcing during the 20th century, *Nat. Geosci.*,  
834 2, 294–300, 2009.

835 Shindell, D. and Faluvegi, G.: The net climate impact of coal-fired power plant emissions, *Atmos. Chem. Phys.*, 10,  
836 3247–3260, <https://doi.org/10.5194/acp-10-3247-2010>, 2010.

837 Shindell D., Kuylenstierna J.C.I., Vignati E., van Dingenen R., Amann M., Klimont Z., Anenberg S.C., Muller N.,  
838 JanssensMaenhaut G., Raes F., Schwartz J., Faluvegi G., Pozzoli L., Kupiainen K., Höglund–Isaksson L.,  
839 Emberson L., Streets D., Ramanathan V., Hicks K., Kim Oanh N.T., Milly G., Williams M., Demkine W.,  
840 Fowler D.: Simultaneously Mitigating Near-Term Climate Change and Improving Human Health and Food  
841 Security. *Science*, Vol. 335, 183–189, 2012.

842 Shindell, D. T., Chin, M., Dentener, F., Doherty, R. M., Faluvegi, G., Fiore, A. M., Hess, P., Koch, D. M.,  
843 MacKenzie, I. A., Sanderson, M. G., Schultz, M. G., Schulz, M., Stevenson, D. S., Teich, H., Textor, C., Wild,  
844 O., Bergmann, D. J., Bey, I., Bian, H., Cuvelier, C., Duncan, B. N., Folberth, G., Horowitz, L. W., Jonson, J.,  
845 Kaminski, J. W., Marmor, E., Park, R., Pringle, K. J., Schroeder, S., Szopa, S., Takemura, T., Zeng, G., Keating,  
846 T. J., Zuber, A.: A multi-model assessment of pollution transport to the Arctic, *Atmos. Chem. Phys. Discuss.*,  
847 2008.

848 Shindell, D. T., Faluvegi, G., Rotstajn, L., and Milly, G.: Spatial patterns of radiative forcing and surface  
849 temperature response, *J. Geophys. Res.-Atmos.*, 120, 5385–5403, <https://doi.org/10.1002/2014JD022752>,  
850 2015.

851 Shindell, D. T., Lamarque, J.–F., Schulz, M., Flanner, M., Jiao, C., Chin, M., Young, P. J., Lee, Y. H., Rotstajn, L.,  
852 Mahowald, N., Milly, G., Faluvegi, G., Balkanski, Y., Collins, W. J., Conley, A. J., Dalsoren, S., Easter, R.,  
853 Ghan, S., Horowitz, L., Liu, X., Myhre, G., Nagashima, T., Naik, V., Rumbold, S. T., Skeie, R., Sudo, K.,  
854 Szopa, S., Takemura, T., Voulgarakis, A., Yoon, J.–H., and Lo, F.: Radiative forcing in the ACCMIP historical

855 and future climate simulations, *Atmos. Chem. Phys.*, 13, 2939–2974, 2013.

856 Shindell, D. T., Voulgarakis, A., Faluvegi, G., and Milly, G.: Precipitation response to regional radiative forcing,  
857 *Atmos. Chem. Phys.*, 12, 6969–6982, doi:10.5194/acp-12-6969-2012, 2012.

858 Smith, S.J. and Mizrahi, A.: Near-term climate mitigation by short-lived forcers. *PNAS* 14202–14206, doi:  
859 10.1073/pnas.1308470110, 2013.

860 Sobhani, N., Kulkarni, S., Carmichael, G. R.: Source sector and region contributions to black carbon and PM<sub>2.5</sub> in  
861 the Arctic. *Atmos. Chem. Phys.*, 18, 18123–18148, 2018.

862 Stjern, C. W., Samset, B. H., Myhre, G., Bian, H., Chin, M., Davila, Y., Dentener, F., Emmons, L., Flemming, J.,  
863 Haslerud, A. S., Henze, D., Jonson, J. E., Kucsera, T., Lund, M. T., Schulz, M., Sudo, K., Takemura, T., and  
864 Tilmes, S.: Global and regional radiative forcing from 20 % reductions in BC, OC and SO<sub>4</sub> – an HTAP2  
865 multi-model study, *Atmos. Chem. Phys.*, 16, 13579–13599, <https://doi.org/10.5194/acp-16-13579-13599>,  
866 2016.

867 Stjern, C. W. et al. Rapid adjustments cause weak surface temperature response to increased black carbon  
868 concentrations. *Geophys. Res.* 122, 11462–11481, 2017.

869 Stohl, A.: Characteristics of atmospheric transport into the Arctic troposphere, *J. Geophys. Res.*, 111, D11306,  
870 <https://doi.org/10.1029/2005JD006888>, 2006.

871 Stohl A., Aamaas B., Amann M., Baker L. H., Bellouin N., Berntsen T. K., Boucher O., Cherian R., Collins W.,  
872 Daskalakis N., Dusinska M., Eckhardt S., Fuglestedt J. S., Harju M., Heyes C., Hodnebrog Ø., Hao J., Im U.,  
873 Kanakidou M., Klimont Z., Kupiainen K., Law K. S., Lund M. T., Maas R., MacIntosh C. R., Myhre G.,  
874 Myriokefalitakis S., Olivie D., Quaas J., Quennehen B., Raut J.-C., Rumbold S. T., Samset B. H., Schulz M.,  
875 Seland Ø., Shine K. P., Skeie R. B., Wang S., Yttri K. E., and Zhu T.: Evaluating the climate and air quality  
876 impacts of short-lived pollutants. *Atmos. Chem. Phys.*, 15, 10529 – 10566, 2015.

877 Stohl, A., Eckhardt, S., Forster, C., James, P., and Spichtinger, N.: On the pathways and timescales of  
878 intercontinental air pollution transport, *J. Geophys. Res.–Atmos.*, 107, ACH 6–1–ACH 6–17,  
879 <https://doi.org/10.1029/2001JD001396>, 2002.

880 Stohl, A., Klimont, Z., Eckhardt, S., Kupiainen, K., Shevchenko, V. P., Kopeikin, V. M., and Novigatsky, A. N.:  
881 Black carbon in the Arctic: the underestimated role of gas flaring and residential combustion emissions, *Atmos.*  
882 *Chem. Phys.*, 13, 8833–8855, <https://doi.org/10.5194/acp-13-8833-2013>, 2013

883 Sudo, K., Sekiya, T., Nagashima, T.: CHASER/MIROC-ESM in HTAP2 status reports, HTAP2 Global and  
884 Regional Model Evaluation Workshop, Nagoya University, JAMSTEC, NIES, 2015.

885 Sudo, K., Takahashi, M., Kurokawa, J.-I., and Akimoto, H.: CHASER: A global chemical model of the troposphere  
886 1. Model description, *J. Geophys. Res.–Atmos.*, 107, ACH 7–1–ACH 7–20, doi:10.1029/2001JD001113,  
887 2002.

888 Søvde, O. A., Prather, M. J., Isaksen, I. S. A., Berntsen, T. K., Stordal, F., Zhu, X., Holmes, C. D., and Hsu, J.: The  
889 chemical transport model Oslo CTM3, *Geosci. Model Dev.*, 5, 1441–1469, doi:10.5194/gmd-5-1441-2012,  
890 2012.

891 Takemura, T., and Suzuki, K.: Weak global warming mitigation by reducing black carbon emissions, *Scientific*  
892 *Reports*, 9, 10.1038/s41598-019-41181-6, 2019.

893 Tan, J., Fu, J. S., Dentener, F., Sun, J., Emmons, L., Tilmes, S., Sudo, K., Flemming, J., Jonson, J. E., Gravel, S.,  
894 Bian, H., Davila, Y., Henze, D. K., Lund, M. T., Kucsera, T., Takemura, T., and Keating, T.: Multi-model study  
895 of HTAP II on sulfur and nitrogen deposition, *Atmos. Chem. Phys.*, 18, 6847–6866, 2018a.

896 Tan, J., Fu, J. S., Dentener, F., Sun, J., Emmons, L., Tilmes, S., Flemming, J., Takemura, T., Bian, H., Zhu, Q., Yang,  
897 C.-E., and Keating, T.: Source contributions to sulfur and nitrogen deposition – an HTAP II multi-model study  
898 on hemispheric transport, *Atmos. Chem. Phys.*, 18, 12223–12240, 2018b.

899 Teng, H., Washington, W. M., Branstator, G., Meehl, G. A., and Lamarque, J.-F.: Potential impacts of Asian carbon

900 aerosols on future US warming, *Geophys. Res. Lett.*, 39, L11703, doi:10.1029/2012GL051723, 2012.

901 Tilmes, S., Lamarque, J.-F., Emmons, L. K., Kinnison, D. E., Marsh, D., Garcia, R. R., Smith, A. K., Neely, R. R.,  
902 Conley, A., Vitt, F., Val Martin, M., Tanimoto, H., Simpson, I., Blake, D. R., and Blake, N.: Representation of  
903 the Community Earth System Model (CESM1) CAM4-chem within the Chemistry- Climate Model Initiative  
904 (CCMI), *Geosci. Model Dev.*, 9, 1853–1890, doi:10.5194/gmd-9-1853-2016, 2016.

905 Twomey, S.: The influence of pollution on the shortwave albedo of clouds, *J. Atmos. Sci.*, 34, 1149–1152, 1977.

906 UNEP/WMO: Integrated Assessment of Black Carbon and Tropospheric Ozone, Nairobi, Kenya, available at:  
907 <http://wedocs.unep.org/handle/20.500.11822/8028> (last access: 13 May 2020), 2011.

908 US EPA: Guidance on the use of models and other analyses for demonstrating attainment of air quality goals for  
909 ozone, PM<sub>2.5</sub>, and regional haze. U.S. Environmental Protection Agency Office of Air Quality Planning and  
910 Standards Air Quality Analysis Division Air Quality Modeling Group Research Triangle Park, NC, 2007.

911 Zhang, H. Y., Cheng, S. Y., Yao, S., Wang, X. Q., and Zhang, J. F.: Multiple perspectives for modeling regional  
912 PM<sub>2.5</sub> transport across cities in the Beijing–Tianjin–Hebei region during haze episodes, *Atmos. Environ.*, 212,  
913 22–35, <https://doi.org/10.1016/j.atmosenv.2019.05.031>, 2019.

914 Zhang, X., Zhang, Y. H., Han, J. B., Zhang, L., and Shi, W. R.: Analysis of the climatic characteristics of the  
915 atmospheric boundary layer height in yanmayan Island, Arctic (in Chinese), *Polar studies*, 30(02):132–139,  
916 2018.